海の研究（Oceanography in Japan），32（3, 4），67－93，2023，doi: 10.5928/kaiyou.32.3-4_67

— 2019年度日本海洋学会賞受賞記念論文 —

Observational and theoretical studies on the North Pacific upper ocean circulation and its variability*

Bo Qiu†

Abstract

This article reviews the four major circulation systems in the wind-driven subtropical gyre of the western North Pacific Ocean: the North Equatorial Current in the southern limb of the gyre, the Subtropical Countercurrent traversing the gyre center latitudes, the bimodal Kuroshio paths south of Japan, and the Kuroshio Extension as the gyre outflow into the open North Pacific Ocean. Although each of these circulation systems has its unique properties and time-varying signals, cases are made that it is dynamically beneficial to consider them in an inter-connected way through external forcings or mutual interactions. Rather than passively responding to the external forcings, such as that related to the Pacific decadal oscillations, it is emphasized that the low-frequency Kuroshio/KE variability can feedback to the overlying atmospheric storm-tracks and form a coupled feedback loop that enhances the decadal variance in the midlatitude North Pacific ocean-atmosphere system.

Key words: Wind-forced circulation variability, Pacific Decadal Oscillation, Midlatitude ocean-atmosphere coupling, Delayed negative feedback

1. Introduction

Following the launch of the TOPEX/Poseidon (T/P) mission in 1992, nadir-looking satellite altimetry has revolutionized how ocean research is conducted. The maturity of the satellite altimetry technology and the 30-year accumulation of the high-quality sea surface height (SSH) data from the subsequent missions (i.e., the T/P Extended Mission, Jason-1, Jason-2, Jason-3, and Jason-CS/Sentinel-6 missions) have provided the research community with an unprecedented opportunity to investigate detailed evolutions of the global and regional ocean circulation and sea level changes from weekly to decadal timescales. Two research areas that have achieved significant advances are the oceanic mesoscale eddy variability and the multi-scale changes in the large-scale ocean circulation.

Acting as an oceanic analogue of atmospheric storms, the oceanic mesoscale variations with horizontal wavelengths of 100-500 km are the most energetic form of flow fluctuations in the world ocean (e.g., Roemmich

* Received 14 June 2023: Accepted 12 July 2023

† Department of Oceanography, University of Hawaii at Manoa, 1000 Pope Rd., Honolulu, HI 96822, USA
Email address for correspondence: bo@soest.hawaii.edu

and Gilson, 2001; Ferrari and Wunsch, 2009; Chelton *et al.*, 2011; Zhang *et al.*, 2014; among others). Although mesoscale variations have been detected prior to the satellite altimetry era, it is not until the establishment of sustained satellite altimetry measurements that they are now being systematically observed on a globally repetitive basis. With the use of SSH data from combined satellite altimeters, we have now a much improved knowledge not only about the global statistical characteristics of the mesoscale eddies (such as their sizes, polarities, and propagation speeds/directions), but also how eddies interact among themselves, the roles they play in determining the surface ocean energetics, and the contributions they make to the transports of heat, salt and other biogeochemical tracers. Satellite altimetry is also aptly suited for exploring the time-varying signals of the large-scale ocean circulation with length scales > O(500 km). Indeed, thanks to the multi-decadal, high-precision, SSH data from various altimetry missions, a rich literature is now available that has delved into lateral movement and strength changes of major oceanic currents, structural changes of the wind-driven tropical, subtropical and subpolar gyres, and regional sea level changes that accompany the low-frequency fluctuations of the oceanic currents and wind-driven gyres (e.g., Imawaki *et al.*, 2013; Stammer *et al.*, 2013; Kida *et al.*, 2015; among others).

Figures 1a and 1b compare the root-mean-squared SSH signals with timescales shorter versus longer than 2 years in the world ocean based on the AVISO merged SSH data. Thus delineated, Fig. 1a reflects largely the regional distribution of mesoscale eddy variability, whereas Fig. 1b represents that of the large-scale ocean circulation variability. Notice that regions with enhanced mesoscale eddy variability often coincide with the regions of elevated large-scale ocean circulation variability. In the North Pacific Ocean, for example, such regions include the Kuroshio/Kuroshio Extension (KE) regions south/east of Japan, the North Equatorial Current (NEC) region east of the Philippines, and the tropical instability wave (TIW) band in the eastern Pacific along ~ 2°N. Dynamically, the ocean circulation variability is multi-scaled and there exist no energy spectral gaps between the meso- and large-scales. Changes in the large-scale major currents and gyres can change the instability threshold, impacting thereby on generation of mesoscale eddies. Likewise, modulations in the mesoscale eddy field can feedback onto the broader-scale oceanic current through nonlinear rectifications. In addition to the cross-scale interactions within a geographic domain, changes in one current system can also exert influences upon neighboring circulation and current systems. After all, demarcations among different current systems in the wind-driven North Pacific subtropical gyre (e.g., that between the Kuroshio and the KE) are a subjective construction.

While it is customary in the past to examine the variability of each current system individually, an objective of this article is to advocate for the need/benefit of exploring the overall wind-driven gyre circulation variability via an inter-connected approach. Specifically, rather than exploring the variability of the NEC in the tropics, the Subtropical Countercurrent (STCC) east Taiwan, and the Kuroshio/KE surrounding Japan (Fig. 2a) independently, it is beneficial to elucidate their variability as an interlinked system. It is argued that an inter-connected approach becomes increasingly more desired when our interest in the circulation variability extends into the decadal-and-longer timescales. To fully elucidate the roles of the North Pacific subtropical gyre variability in the climate system, it is further argued in this article that there is a need to elucidate the ocean-atmosphere coupling involving the Kuroshio/KE variability and the overlying atmospheric storm-tracks across the mid-latitude North Pacific basin.

2. The North Equatorial Current

The southern limb of the wind-driven subtropical gyre in the North Pacific is carried by the west-

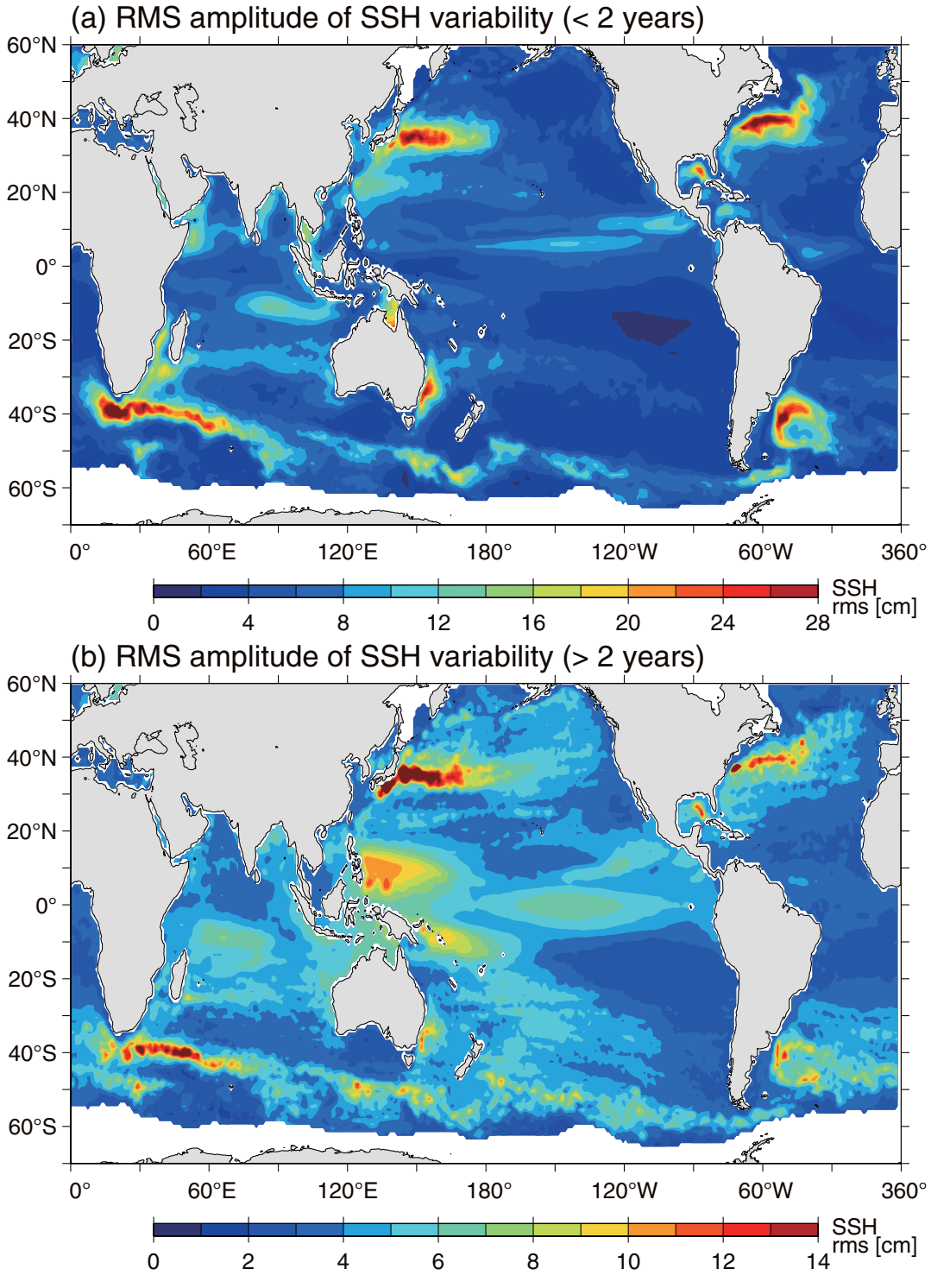

Fig. 1. (a) Root-mean-squared (rms) SSH signals in the Pacific Ocean, based on high-pass-filtered AVISO SSH data from January 1993 to December 2022. The high-pass filter has a half-power at 1.5 years. (b) Same as (a) except for the low-pass-filtered SSH signals. Thus filtered, (a) represents the oceanic mesoscale eddy variability and (b) the large-scale oceanic circulation/ sea level variations.

ward-flowing NEC whose center latitude is located at ~ 13°N in the northwestern Pacific basin (Fig. 2b). This latitude corresponds closely to the mean zero wind-stress curl line across the North Pacific Ocean (Risien and Chelton, 2008). Upon reaching the Philippine coast along 125°E, the NEC bifurcates (pink dot in Fig. 2b), with one portion of it turning poleward to form the Kuroshio and the rest veering equatorward to feed the Mindanao Current. The NEC's bifurcation and variability and are subject to both the local monsoonal wind forcing and the remote forcing across the broad interior ocean via the propagation by wind-forced baroclinic Rossby waves (Qiu and Lukas, 1996; Kim *et al.*, 2004; Qiu and Chen 2012).

Figure 3a shows the monthly time series of the NEC bifurcation latitude Y_b(t) along the Philippine coast. It is defined by the location of zero meridional geostrophic velocity estimated from the gridded altimetric SSH dataset (Qiu and Chen, 2010a). While exhibiting variability with time scales ranging from intra-seasonal to decadal, the observed Y_b(t) is clearly dominated by the interannual and longer time-scale fluctuations. To better understand the multi-scaled variability of the NEC bifurcation, it is helpful to recognize that the Y_b(t) time series has a high *negative* correlation ($R \simeq -0.85$) with the anomalous SSH signals in the region neighboring the NEC bifurcation (Fig. 3b). Dynamically, this high correlation makes sense because SSH would drop (increase) if the NEC migrates poleward (equatorward) and brings northward (southward) the tropical low-SSH (subtropical high-SSH) water (recall the mean SSH map of Fig. 2b). Indeed, a comparison between Y_b(t) and the SSH anomaly time series in the 12°-14°N, 127°-130°E box (Fig. 3c) reveals that the latter captures favorably the interannual-to-decadal fluctuations in Y_b(t). In other words, the SSH variability in this key box off the Philippine coast serves as an excellent proxy for the low-frequency changes in the NEC bifurcation and exploring the NEC bifurcation changes becomes equivalent to clarifying the causes underlying the anomalous SSH signals off the Philippines.

It is well established by now that the low-frequency SSH variations in an open ocean are governed by the linear vorticity equation in a 1.5-layer reduced gravity model (see Qiu, 2002, for the derivation and relevant references):

$$\frac{\partial \eta}{\partial t} - C_R \frac{\partial \eta}{\partial x} = -\frac{g'}{g} \nabla \times \left(\frac{\tau}{\rho_0 f} \right) - \varepsilon \eta \qquad (1)$$

where η is the SSH anomaly of our interest, C_R the long baroclinic Rossby wave speed (Chelton *et al.*, 2008), g' the reduced gravity, f the Coriolis parameter, ρ_0 the reference density, τ the anomalous wind stress vector, and ε the Newtonian dissipation rate. The blue line in Fig. 3d shows the η time series in the 12°-14°N, 127°-130°E box based on Eq. (1) and the European Centre for Medium-Range Weather Forecasts (ECMWF) ERA-5 reanalysis wind stress data. It reproduces favorably the observed SSH signals, or the Y_b(t) time series (black line in Fig. 3d), confirming that the low-frequency variability of the NEC bifurcation in the western Pacific Ocean is largely wind forced. Several physical insights can be gained from the linear vorticity model of Eq. (1). First, despite the large meridional excursion with an annual amplitude exceeding 10° latitudes in the zero wind stress curl line across the North Pacific basin, the annual variation in Y_b(t), as shown in Fig. 3a, is weak with an amplitude < 1° latitude. This lack of Y_b(t) response to the annual wind stress curl variability is due to the fact that the SSH response in Eq. (1) acts as an integrator to the wind stress curl forcing along the baroclinic Rossby wave characteristic. As it takes ~ 3.4 years for the baroclinic Rossby waves to transverse the North Pacific basin along 13°N, the effect by the strong annual wind stress curl forcing is integrated out, resulting in weak annual fluctuations in Y_b(t).

Second, validity of the linear vorticity model allows us to hindcast the SSH changes backward in time by using the available reanalysis wind stress product. Given the result of Fig. 3d, the linear vorticity model pro-

vides us with a framework to infer the NEC bifurcation variability over the time period beyond the satellite altimeter era. Figures 4a shows the inferred $Y_b(t)$ changes since 1952 based on the ECMWF ERA-5 dataset

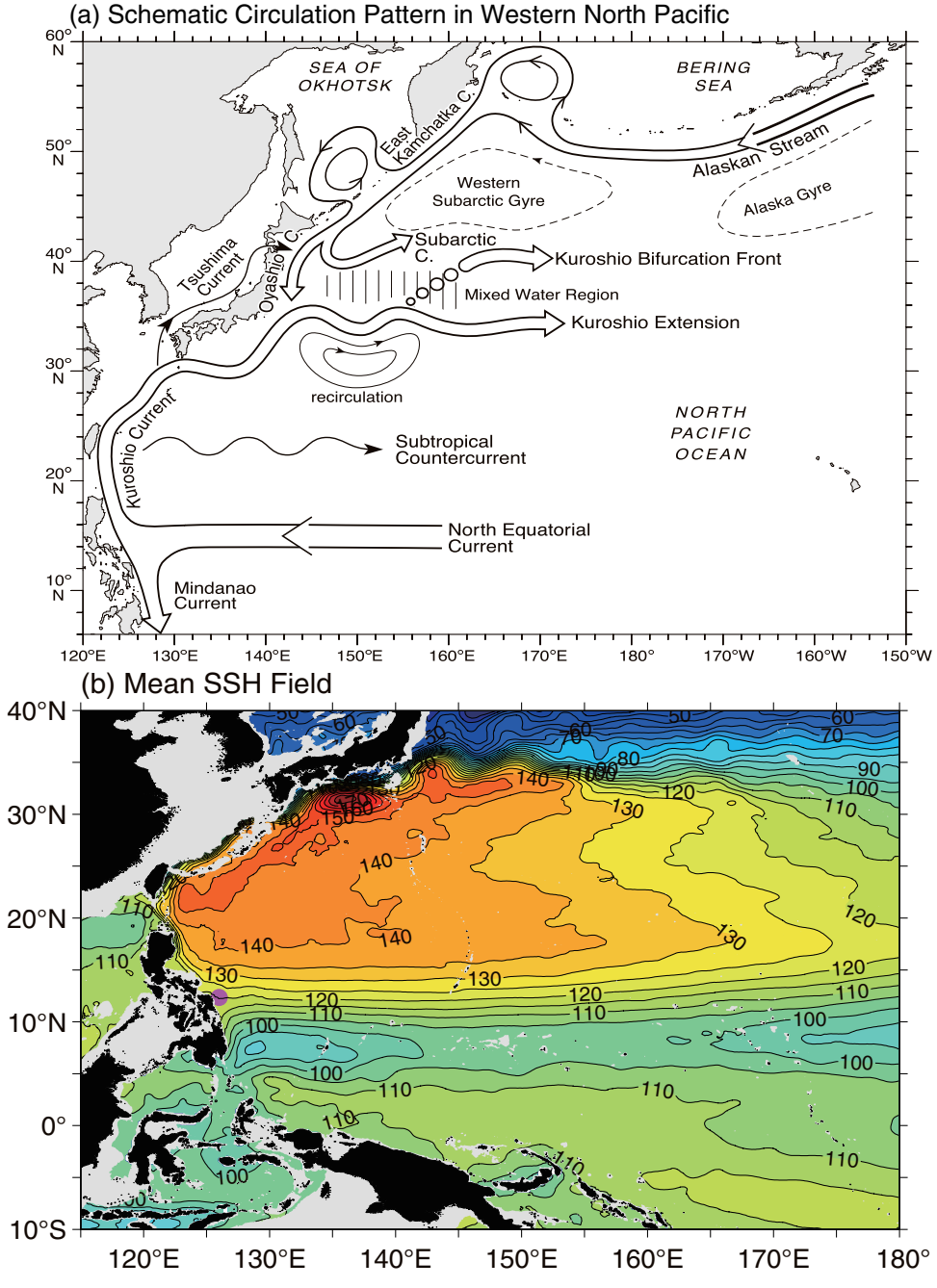

Fig. 2. (a) Schematic upper ocean circulation patterns in the western North Pacific. Adapted from Qiu (2019). (b) Mean sea surface height field (cm) of the western North Pacific from Jousset *et al.* (2022). Gray shades denote where water depth is shallower than 1,000 m. The pink dot near 13°N along the Philippine coast indicates the mean location of the NEC bifurcation.

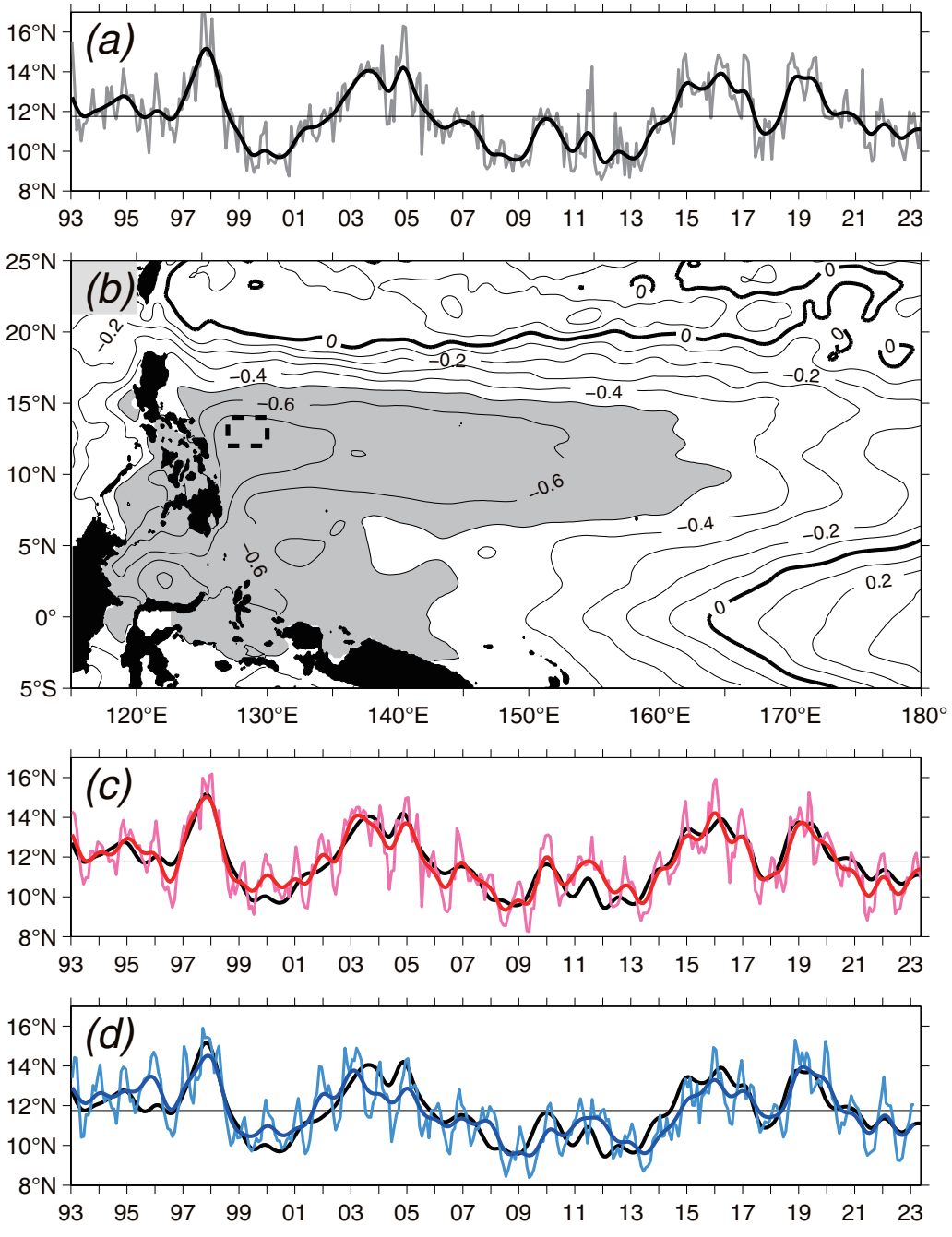

Fig. 3. (a) Time series of the NEC bifurcation latitude $Y_b(t)$ inferred from the monthly satellite altimeter SSH data (gray line). Black line indicates the low-pass filtered $Y_b(t)$ time series after applying a Gaussian filter with a 12-month decay scale. (b) Linear correlation coefficient between the monthly $Y_b(t)$ and the SSH anomalies. Areas where the correlation coefficient amplitude exceeds 0.5 are shaded. Dashed line denotes the key box for $Y_b(t)$. (c) Red lines denote the observed monthly and low-pass filtered SSH anomaly data in the key box. (d) Blue lines denote the modeled monthly and low-pass filtered SSH anomaly data in the key box based on Eq. (1). In (c) and (d), black lines are the same as that in (a) and the regression equation between the SSH anomalies $h'(t)$ value in cm and $Y_b(t)$ is $Y_b(t) = 11.9 - 0.17\ h'(t)$ [°N].

available after 1950. The low-frequency ocean circulation and sea level variability, including the NEC bifurcation, in the western tropical Pacific is known to be subject to both the El Nino-Southern Oscillation (ENSO) and Pacific decadal oscillation (PDO) forcings (e.g., Qiu and Chen, 2012; Wang *et al.*, 2014; Hu *et al.*, 2015; Capotondi and Qiu, 2023; see Figs. 4b-4c). For the interannual-to-decadal changes in the NEC bifurcation, an interesting aspect is that Y_b(t)'s correlation to the Nino-3.4 index remains largely a constant ($R \simeq 0.6$) over the 1965-2005 period (Fig. 4d). It, however, decreased to $R \simeq 0.4$ over the last 15 years. In contrast, while the PDO forcing had little impact on Y_b(t) prior to 1990, its impact increased steadily after 1990 and surpassed that by ENSO after 2005 (Fig. 4e). Dynamically, this shift between the relative importance of ENSO versus PDO forcings on Y_b(t) is a consequence of the subtle, multi-decadal changes in the PDO-related wind stress curl imprint over the tropical western Pacific Ocean. As shown in Fig. 5a, during the period of 1950-1989, the PDO-related wind stress curl forcing averaged along the NEC bifurcation band of 10°-12°N is close to zero. This forcing pattern is altered in the recent three decades in which the PDO-related forcing has a prominent positive wind stress curl in the 10°-12°N band across the western Pacific Ocean (Fig. 5b). Such a forcing in the positive PDO phase would lower the regional SSH through Ekman divergence and cause the NEC bifurcation to shift poleward. One cause for this shift in the PDO forcing pattern over the western tropical Pacific may be related to the Atlantic Multidecadal Oscillation (AMO) whose phase in the early 1990s shifted from negative to positive (Wu *et al.*, 2019).

It is worth emphasizing that as the NEC bifurcation latitude changes on various timescales, it affects not only the dynamical state of, and the partitioning between, the Kuroshio and the Mindanao Current east of the Philippine coast (Kim *et al.*, 2004; Gordon *et al.*, 2014; Schonau *et al.*, 2022), it also impacts the sea level elevations inside the Sulu and South China Seas via coastal wave guide (Zhuang *et al.*, 2013), and the throughflow from the North Pacific Ocean into the South China Sea through the Luzon Strait (Wu, 2013; Nan *et al.*, 2013). Although we have emphasized in this section the usefulness of linear vorticity model as a dynamical framework, nonlinear processes involving wind-forced baroclinic Rossby waves interacting with the background North Equatorial Countercurrent (NECC) can produce large-amplitude, short-term circulation/SSH fluctuations through barotropic instability in the tropical western Pacific Ocean (Qiu *et al.*, 2019).

3. The Subtropical Countercurrent

In the North Pacific Ocean, the large-scale atmospheric forcing by the midlatitude westerlies and tropical trade winds not only generates the basin-wide subtropical gyre circulation, it also produces meridional Ekman temperature flux convergence along the center latitudes, ~ 18°-28°N, of the subtropical gyre and forms the Subtropical Front (STF) in the upper ocean layer (Roden, 1980; Fig. 6b). Since the wind-driven main thermocline beneath the STF tilts downward towards north, the presence of STF with its isopycnals tilting upward towards north creates an eastward geostrophic shear and an eastward-flowing Subtropical Countercurrent (STCC) in the upper 100-m layer (Yoshida and Kidokoro, 1967; Kubokawa, 1997). Although the mean STCC is a weak flow with an amplitude only a few cm/s as indicated in Fig. 6b, it is highly *baroclinically* unstable due to the change in sign of meridional potential vorticity gradients in the surface STCC layer and the subsurface NEC layer (Qiu, 1999; Roemmich and Gilson, 2001; Kobashi and Kawamura, 2002). Indeed, the STCC band of 18°-28°N is the region with the 3rd highest eddy kinetic energy (EKE) level in the western North Pacific after the Kuroshio/KE and NECC bands (Fig. 6a).

The altimeter-measured EKE level in the STCC band reveals a well-defined annual cycle, as well as large-amplitude interannual-to-decadal modulations

(Fig. 7a). Seasonally, the STCC eddy variability has a maximum in May/June and a minimum in December/January. This seasonal EKE change is the result of seasonal variations in the vertical shear of the horizontal

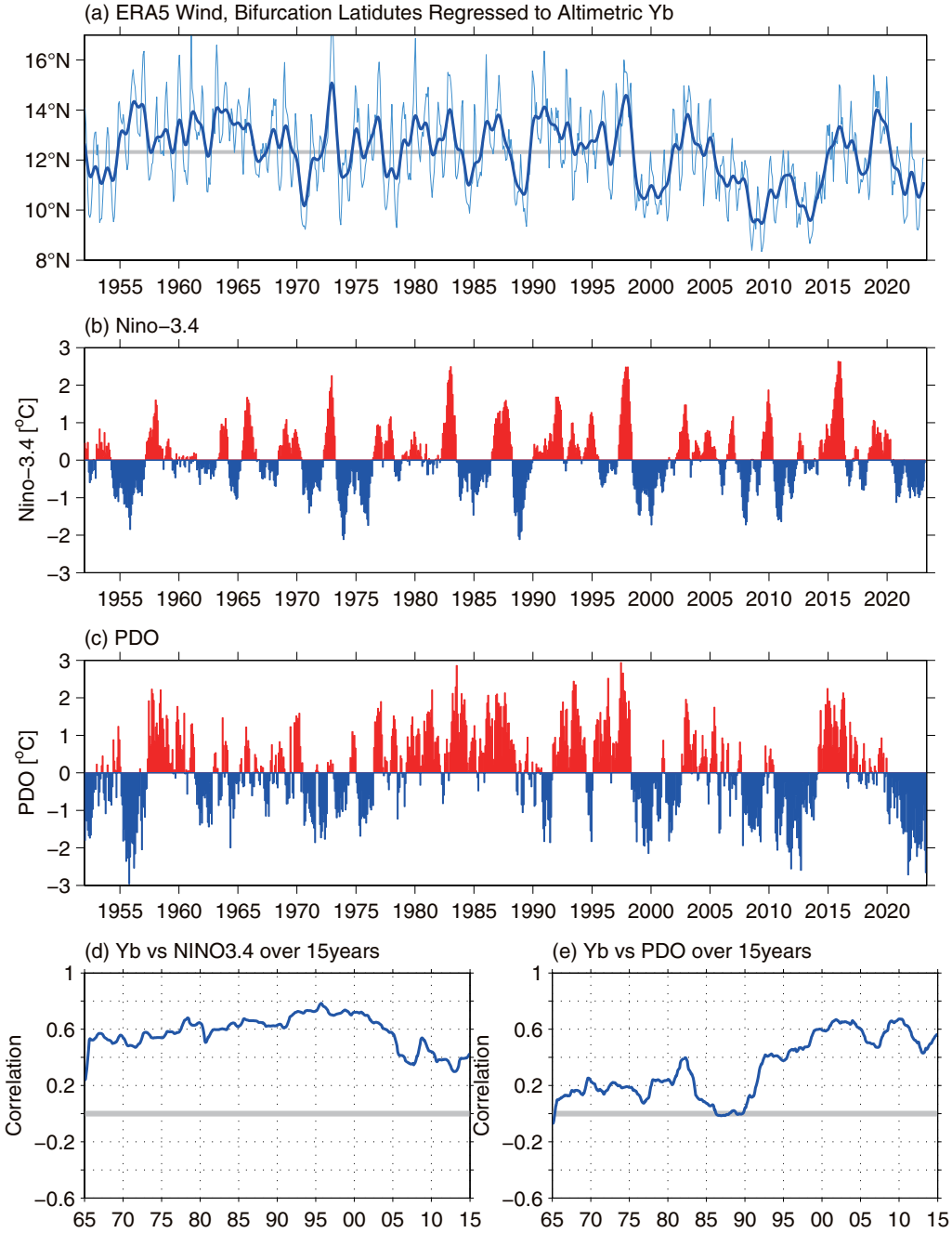

Fig. 4. (a) Time series of the model-inferred NEC bifurcation latitude $Y_b(t)$ based on Eq. (1). Thin (thick) blue line denotes the monthly (low-pass filtered) time series. (b) Time series of Nino-3.4 index. (c) Time series of PDO index. (d) Correlation between $Y_b(t)$ and the Nino-3.4 index as a function of time within a 15-year running time window. (e) Same as (d), but between $Y_b(t)$ and the PDO index.

velocity between the eastward-flowing STCC and the westward-flowing NEC. The STCC-NEC shear reaches a seasonal maximum in late winter (March) when the meridional upper ocean temperature gradient peaks. Based on stability analysis in a vertically-sheared 2.5-layer STCC-NEC system, Qiu (1999) found that the ~ 2-month delay of the EKE maximum observed in the STCC band (in May/June) behind the maximum STCC-NEC shear (in March) is due to the time required for baroclinic instability of the STCC-NEC system to fully grow.

On the interannual and longer timescales, the observed EKE level in the STCC band exhibits a favorable *positive* correlation with the PDO index (cf. Figs.

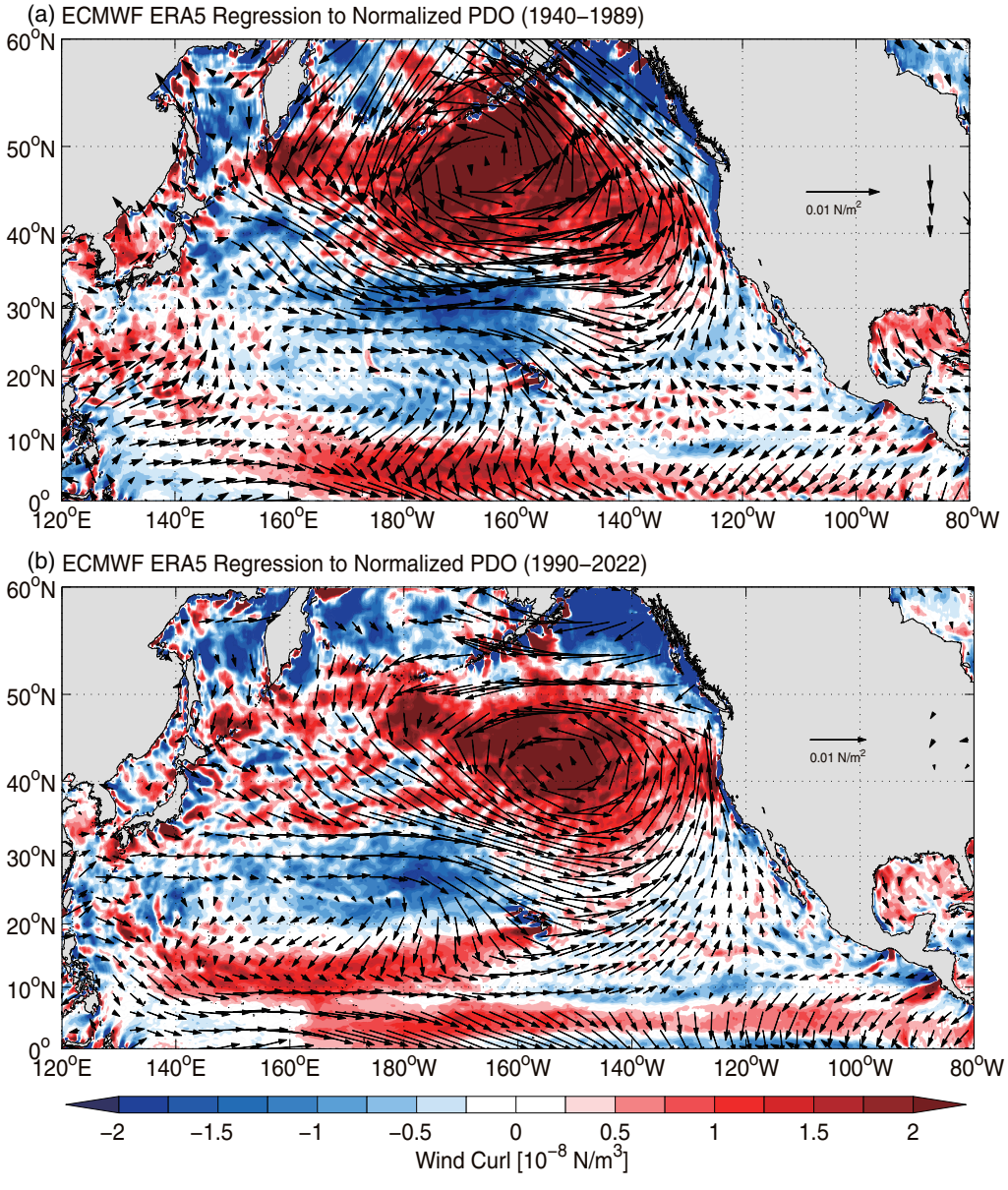

Fig. 5. Surface wind stress vectors and wind curl (in color) patterns regressed to the annually averaged PDO time series in (a) 1940-1989 and (b) 1990-2022 based on the ECMWF ERA-5 reanalysis wind stress dataset.

7a and 7c). This positive correlation stems from the fact that the STCC-NEC shear is controlled by the PDO-related wind stress forcing (Qiu and Chen, 2010b). As shown in Fig. 5, when the PDO forcing is in a positive

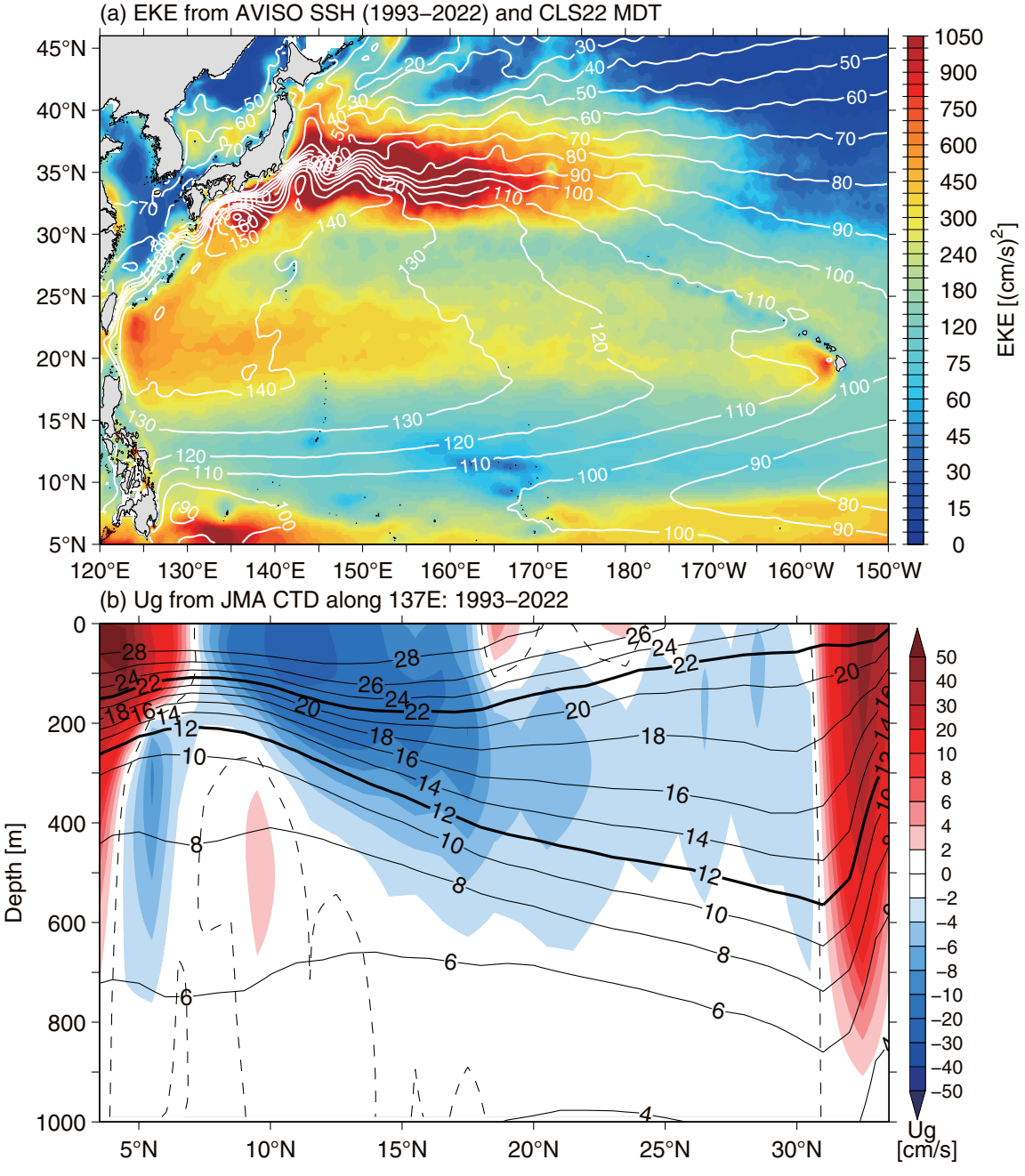

Fig. 6. (a) Eddy kinetic energy distribution in the western North Pacific based on the CMEMS satellite altimeter data from 1993 to 2022. White contours denote the mean SSH by Jousset *et al.* (2022). (b) Latitude-depth section of temperature (solid contours) and zonal geostrophic velocity (color shading) along 137°E from the JMA repeat hydrographic surveys of 1993-2022. Dashed lines denote the zero velocity contours.

phase, both westerlies and trade winds intensify over the North Pacific west of 160°W. This works to enhance the meridional Ekman flux convergence along the STCC band in the western North Pacific (Fig. 7b), increasing the vertical STCC-NEC shear through the thermal wind balance, and the intensity of baroclinic instability and leading to increased regional EKE level. Notice that on decadal timescales, the STCC EKE level in addy-rich years is ~ 300 cm^2/s^2, which is twice as large as the EKE level in eddy-poor years. Spatially, Fig. 8 reveals that the EKE level difference between the different positive vs. negative PDO years is consistent and geographically coherent. This implies the repetitive nature of the PDO-induced stability changes across the STCC-NEC system in the western North Pacific basin (Qiu and Chen, 2013).

After mesoscale eddies are generated along the baroclinically unstable STCC-NEC system, they tend to

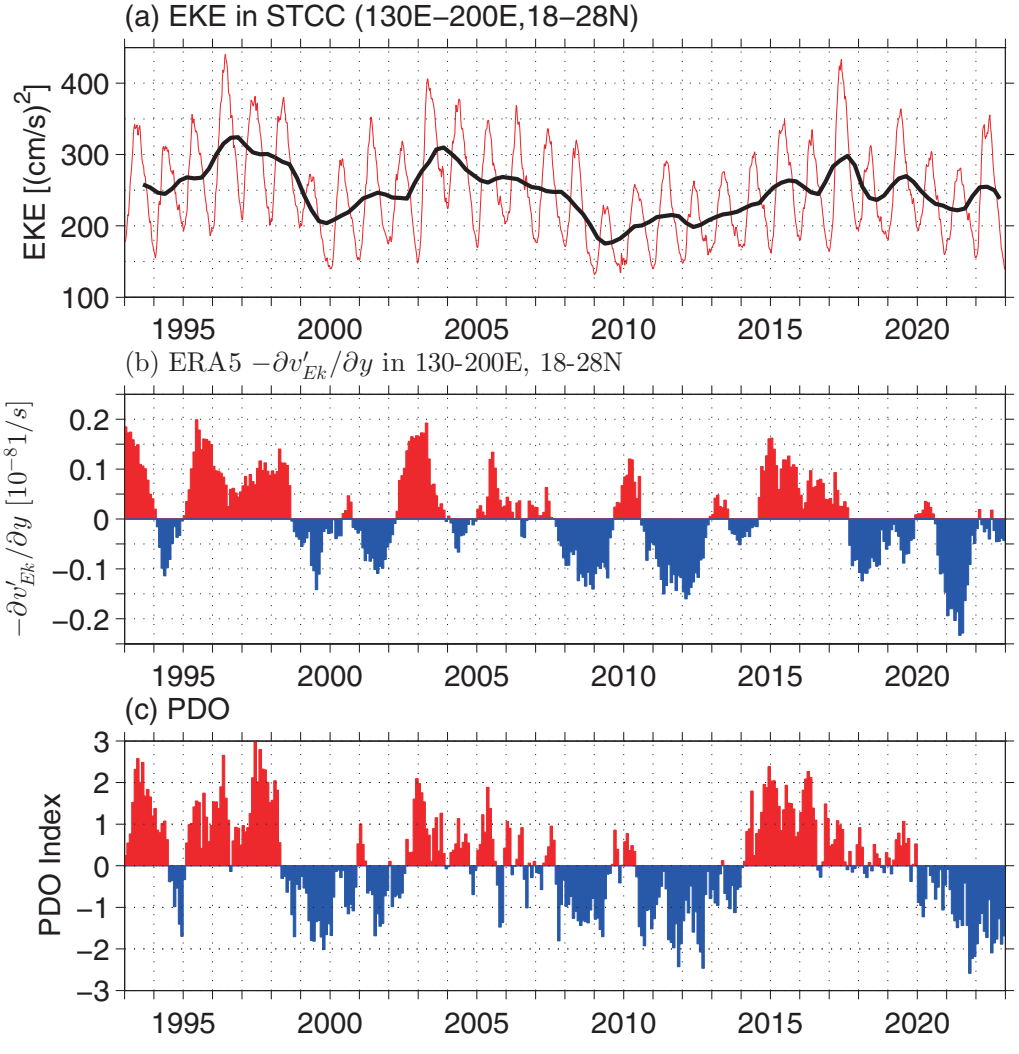

Fig. 7. (a) Eddy kinetic energy time series in the STCC band of 18°-28°N, 130°-200°E. The red line shows the weekly time series and black line the low-pass-filtered time series after applying a Gaussian filter with a 12-month decay scale. (b) Time series of meridional Ekman flux convergence anomalies in the STCC band after removing the climatological seasonal cycle. (c) The PDO index.

propagate westward and accumulate towards the west of the Philippine Sea basin (recall Fig. 6a). In the Philippine Sea, the STCC mesoscale eddies have a dominant period of ~ 100 days and a westward propagating speed of ~ 9 cm/s (Chelton *et al.*, 2011; Qiu and Chen, 2010b). Upon reaching the boundary of the Luzon Strait and Taiwan, the impinging STCC eddies can significantly alter the path and transport of the northward-flowing Kuroshio (Zhang *et al.*, 2001; Gilson and Roemmich, 2002; Hsin *et al.*, 2013). By reducing the

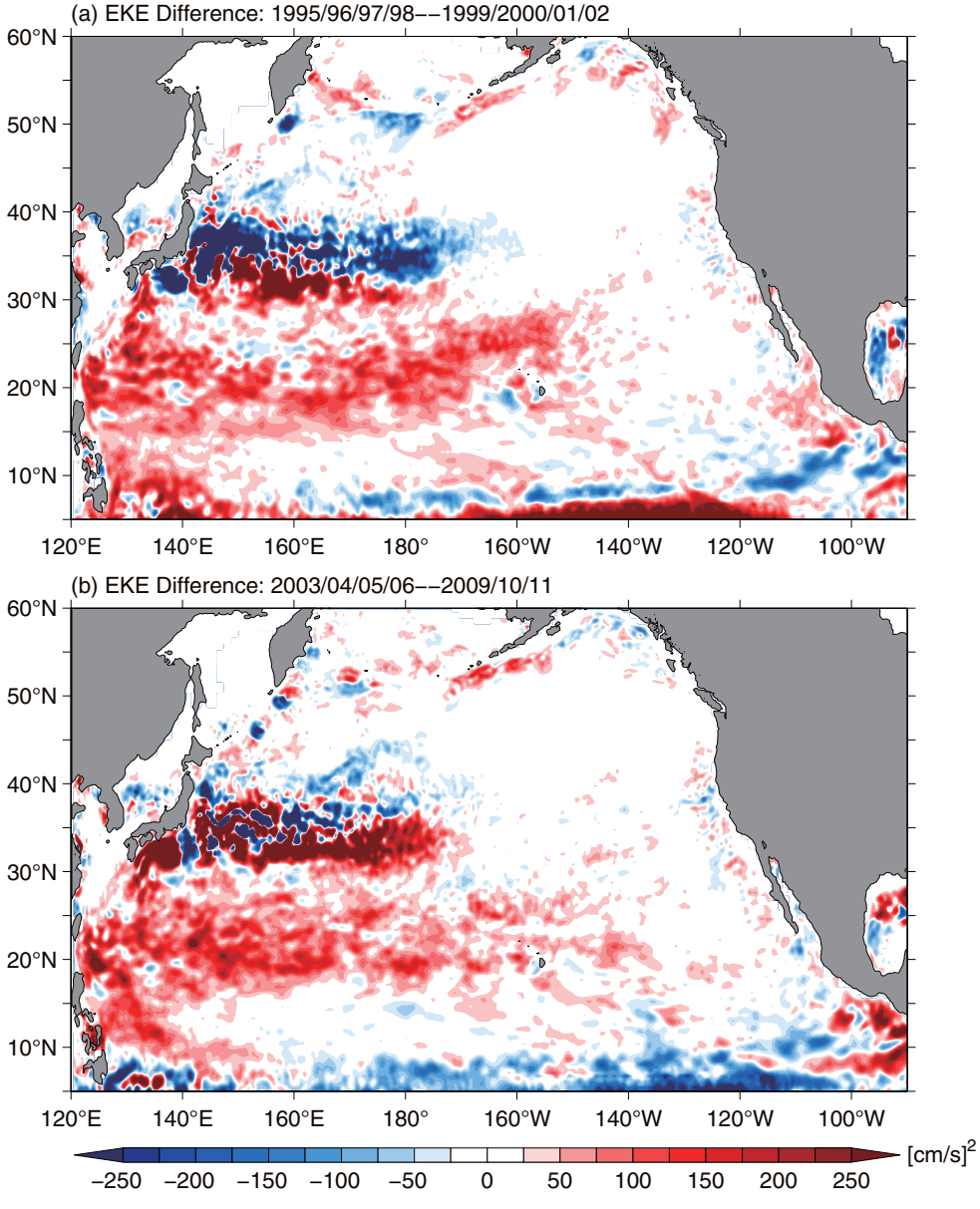

Fig. 8. Difference in eddy kinetic energy level in the North Pacific Ocean between the positive versus negative PDO phase years: (a) 1995-1998 minus 1999-2002 and (b) 2003-2006 minus 2009-2011. Adapted from Fig. 4 in Qiu and Chen (2013).

Kuroshio transport northeast of the Luzon Island, for example, the impinging STCC eddies can facilitate the North Pacific water to enter the South China Sea via formation of intruding eddies (Lien *et al.*, 2014; Zhang *et al.*, 2013). East of Taiwan, instead of flowing due northward into the East China Sea, STCC eddy-Kuroshio interaction can force part of the northward-flowing Kuroshio to divert to east of the Ryukyu Islands and contribute to the formation of the Ryukyu Current (Ichikawa *et al.*, 2004 Andres *et al.*, 2008).

A noticeable result in Fig. 6a, which is heretofore under-appreciated, is that a large portion of the STCC-originated eddy variability is absorbed and transmitted northeastward into the Kuroshio south of Japan along the eastern flank of the Ryukyu Islands. This hints that the low-frequency mesoscale eddy variability originated in the STCC band could affect potentially the low-frequency Kuroshio variability south of Japan. The prominent and widely-known Kuroshio variability south of Japan is its bimodal path fluctuations between straight and large meander (LM) paths. One proxy that captures faithfully this bimodal Kuroshio path changes is the sea level difference measured at the Kushimoto and Uragami tide gauge stations (Kawabe, 1995; Fig. 9a). When the Kuroshio is in a straight-path (LM) state, its in-shore (off-shore) path causes the Kushimoto-Uragami sea level difference to increase (drop). Since 1950, eight LM events have been observed with seemingly random occurrences and widely different durations (see shaded periods in Fig. 9a).

By synthesizing available in situ/satellite observations and atmospheric reanalysis product, Qiu and Chen (2021) sought to elucidate processes conducive for the LM occurrence. They found neither changes in the inflow Kuroshio transport from the East China Sea nor in the downstream KE dynamic state (see section 4 below) were determinant factors. Instead, many existing studies have found that high mesoscale eddy activity originated in the STCC band played critical and inducive roles. For both the 2004 and 2017 LM initiations, satellite altimeter measurements revealed that the increased STCC EKE level favored the generation of cyclonic-anticyclonic eddy pairs: working in tandem, the cyclonic eddy helped to trigger a small-amplitude cyclonic meander of the Kuroshio path southeast of Kyushu and the anticyclonic eddy facilitated the subsequent stalling/growth of the cyclonic-eddy triggered meandering path, leading to full formation of a LM event (Miyazawa *et al.*, 2004; Usui *et al.*, 2008; Qiu *et al.*, 2020).

Statistically, occurrence of this intense cyclonic-anticyclonic eddy interaction is favored when the EKE level along the STCC band is elevated as during the periods prior to the 2004 and 2017 LM events (Fig. 7a). Given the observed STCC EKE level is modulated by the overlying wind stress forcing via Ekman flux convergence (Fig. 7b), it is instructive to examine the long-term changes in the meridional Ekman flux convergence averaged in the STCC band. As shown in Fig. 9b, seven of the past eight LM events after 1950 are found to be preceded by 1-2 years by enhanced *positive* Ekman flux convergent forcings over the STCC. Rather than a fully random phenomenon, Qiu and Chen (2021) posited that the LM occurrence is facilitated by the increased STCC eddy variability that, in turn, is regulated by the regional positive-phased PDO wind stress forcing.

4. The Kuroshio Extension System

The Kuroshio separates from the Japan coast near 140°E, 35°N and, after entering the open North Pacific Ocean, it is renamed the Kuroshio Extension (KE; Fig. 2a). Free from the constraint of coastal boundaries, the KE has been observed to be an eastward-flowing inertial jet accompanied by large-amplitude meanders and energetic pinched-off eddies. In addition to having the highest EKE level in the North Pacific Ocean (Fig. 6a), the KE eddy variability exhibits decadal modulations in connection to its dynamical state fluctuations (Qiu and

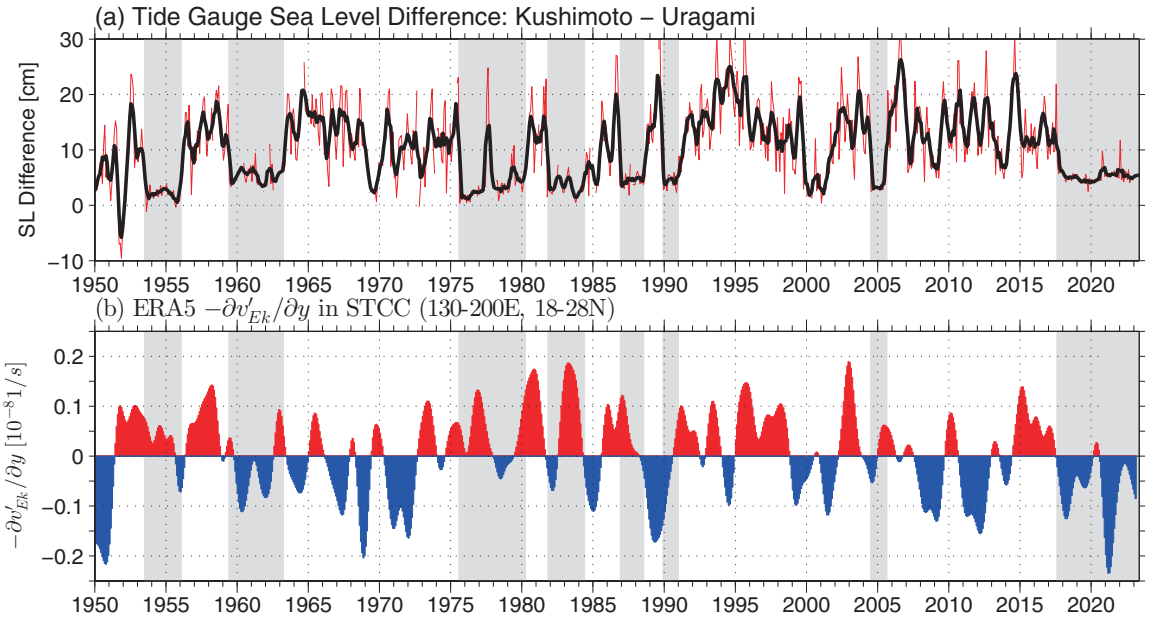

Fig. 9. (a) Monthly time series of sea level difference of Kushimoto-Uragami. Black line denotes the time series after 5-month running mean. Shaded windows denote the Kuroshio large meander periods. (b) Time series of meridional Ekman flux convergence anomalies averaged in the STCC band. Both adapted from Qiu and Chen (2021).

Chen, 2005, 2010c). As shown in Fig. 10, the KE paths were relatively stable in 1993-95, 2002-05, 2010-16, and after 2018. In contrast, spatially convoluted paths prevailed during 1996-2001, 2006-09, and 2016-17. When the KE is in a stable dynamical state, satellite altimeter measurements further reveal that the KE path-length from 141°E to 153°E is shorter, its eastward transport and latitudinal position tend to increase and migrate northward, and its southern recirculation gyre tends to strengthen (Figs. 11a-11d). The reverse is observed when the KE system switches to an unstable dynamical state.

Because these properties of KE are temporally correlated, they can be combined (by reversing the sign of path-length and averaging the 4 timeseries normalized by their respective standard deviations) to form a KE index to succinctly represent the KE's dynamical state (Fig. 11e). Thus formulated, a positive KE index signifies a stable dynamical state and a negative index, an unstable dynamical state. Similar to the Y_b(t) time series constructed for the NEC bifurcation latitude variability, the KE index can be used to relate the decadal KE variability to the regional SSH anomalies and to help identify the forcing processes. Based on a linear correlation analysis similar to those summarized in Fig. 3, the KE index is found to be correlated favorably with the anomalous SSH signals in the KE southern recirculation gyre box of 31°-36°N, 140°-165°E (compare Figs.11e with 11f; Qiu *et al.*, 2014). In other words, exploring the decadal KE variability becomes equivalent to quantifying the SSH changes in the key box of 31°-36°N, 140°-165°E. Using the linear vorticity model, Eq. (1), forced by the ECMWF ERA-5 reanalysis wind stress data, Fig. 11g shows that the SSH anomalies hindcasted in this key box match well with the observed SSH time series in Fig. 11f. This implies that a significant portion of the observed decadal KE variability is forced externally by wind stresses across the

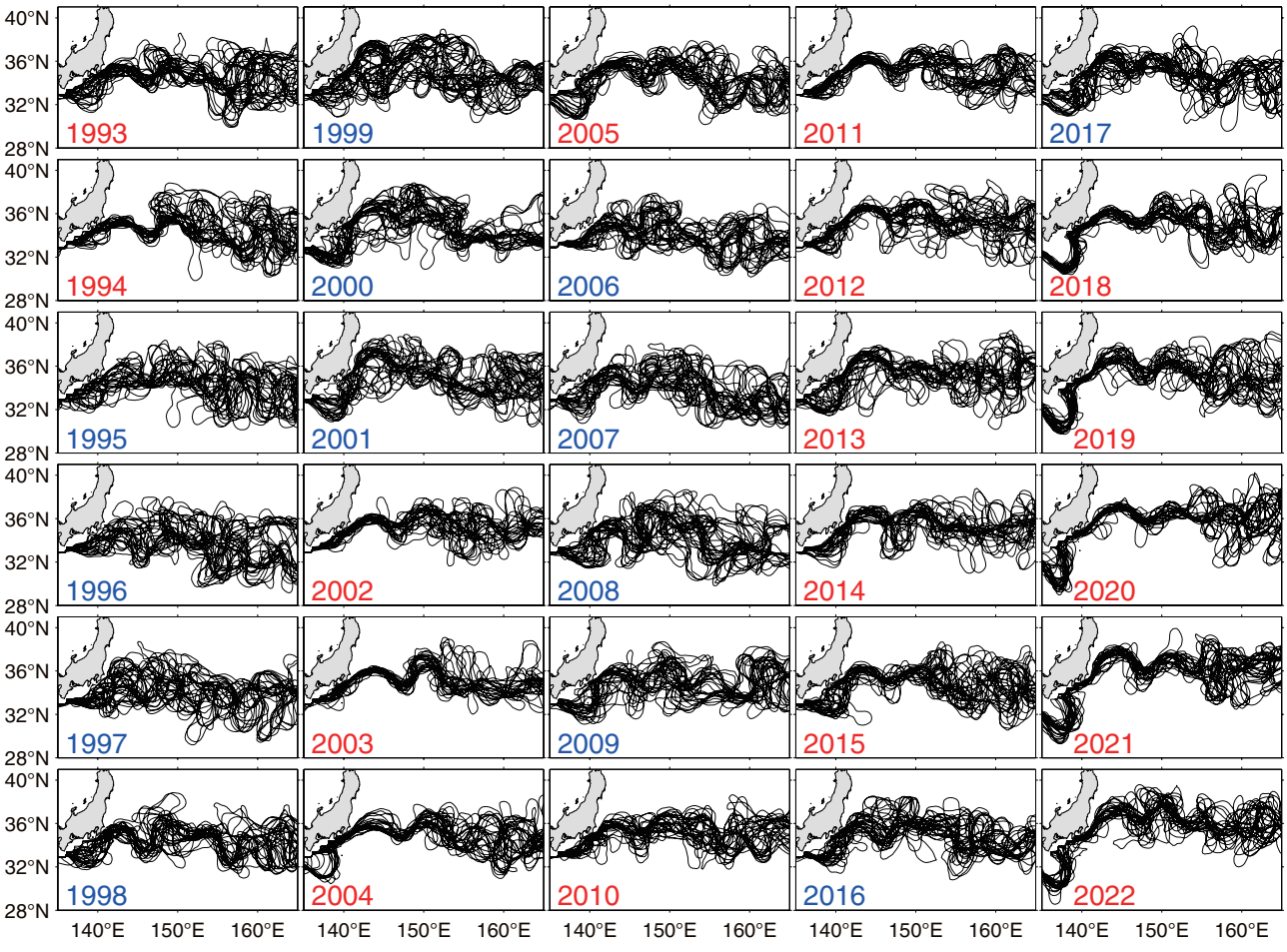

Fig. 10. Yearly paths of the Kuroshio and KE plotted every 14 days since 1993 based on satellite altimetry observations [for detailed path derivation, see Qiu and Chen (2005)]. Red (blue) labels denote years in which the KE is largely in a stable (unstable) dynamic state.

mid-latitude North Pacific basin.

To relate the wind forcing in the 31°-36°N band to the decadal KE variability, it is instructive to notice that the PDO-modulated wind stress curl is positive in the eastern basin of 160°-130°W (recall Fig. 5). A look at the observed SSH anomalies along this band (Figs. 12a-12b) reveals that the transitions between the KE dynamical states are induced by arrivals of SSH anomalies in the KE recirculation gyre that have been generated in the eastern basin. Specifically, when the eastern North Pacific wind stress curl anomalies are positive during the positive PDO phase (Fig. 12c), enhanced Ekman flux divergence generates negative SSH anomalies in 170°-140°W. As these negative SSH anomalies propagate westward as baroclinic Rossby waves into the KE region after a delay of ~ 3 years, they weaken the zonal KE jet, leading to an unstable (i.e., a negative index) state of the KE system with a reduced recirculation gyre and an active eddy kinetic energy field. Negative anomalous wind stress curl forcing during the negative PDO phase, on the other hand, generates positive SSH anomalies through the Ekman flux convergence in the eastern North Pacific. After propagating into the KE region in the west, these

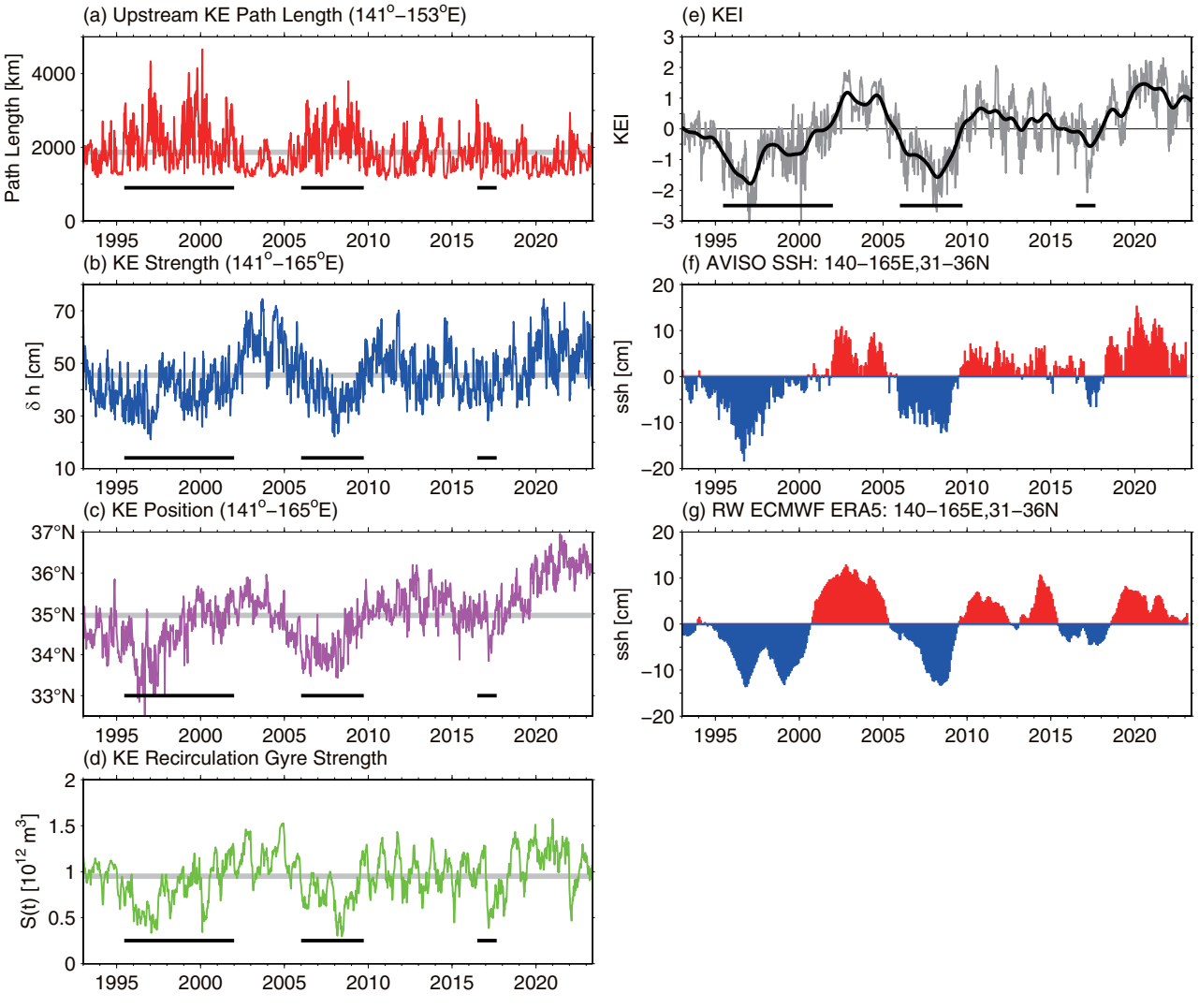

Fig. 11. Time series of (a) KE pathlength integrated from 141° to 153°E, (b) SSH difference across the KE jet from 141° to 165°E, (c) latitudinal KE position from 141° to 165°E, (d) intensity of the KE recirculation gyre, and (e) synthesized KE index. Black bars denote the periods when the KE is in unstable state. Thick black line in (e) shows the low-passed KE index by a Gaussian filter with a 4-month decay scale. (f) Altimeter-observed SSH anomaly time series in the key KE box of 31°-36°N, 140°-165°E. (g) SSH anomaly time series hindcasted by the linear vorticity model, Eq. (1), based on ERA-5 reanalysis wind stress data.

anomalies stabilize the KE system by increasing the KE transport and by shifting its position northward, leading to a positive index state. Notice that the relationship between the KE dynamical state change and the wind stress forcing in the eastern North Pacific basin has been elaborated by many existing modeling and data analysis studies (e.g., Taguchi *et al.*, 2007; Sugimoto and Hanawa, 2009; Ceballos *et al.*, 2009; Sasaki *et al.*, 2013; Pierini, 2014; Nonaka *et al.*, 2020).

By merging the ECMWF reanalysis wind stress product ERA-20C (available from 1900 to 2010; Stickler *et al.*, 2014) and ERA-5 and forcing the 1.5-layer reduced-gravity model Eq. (1), we can extend the SSH-based KE index time series backward in time to 1905

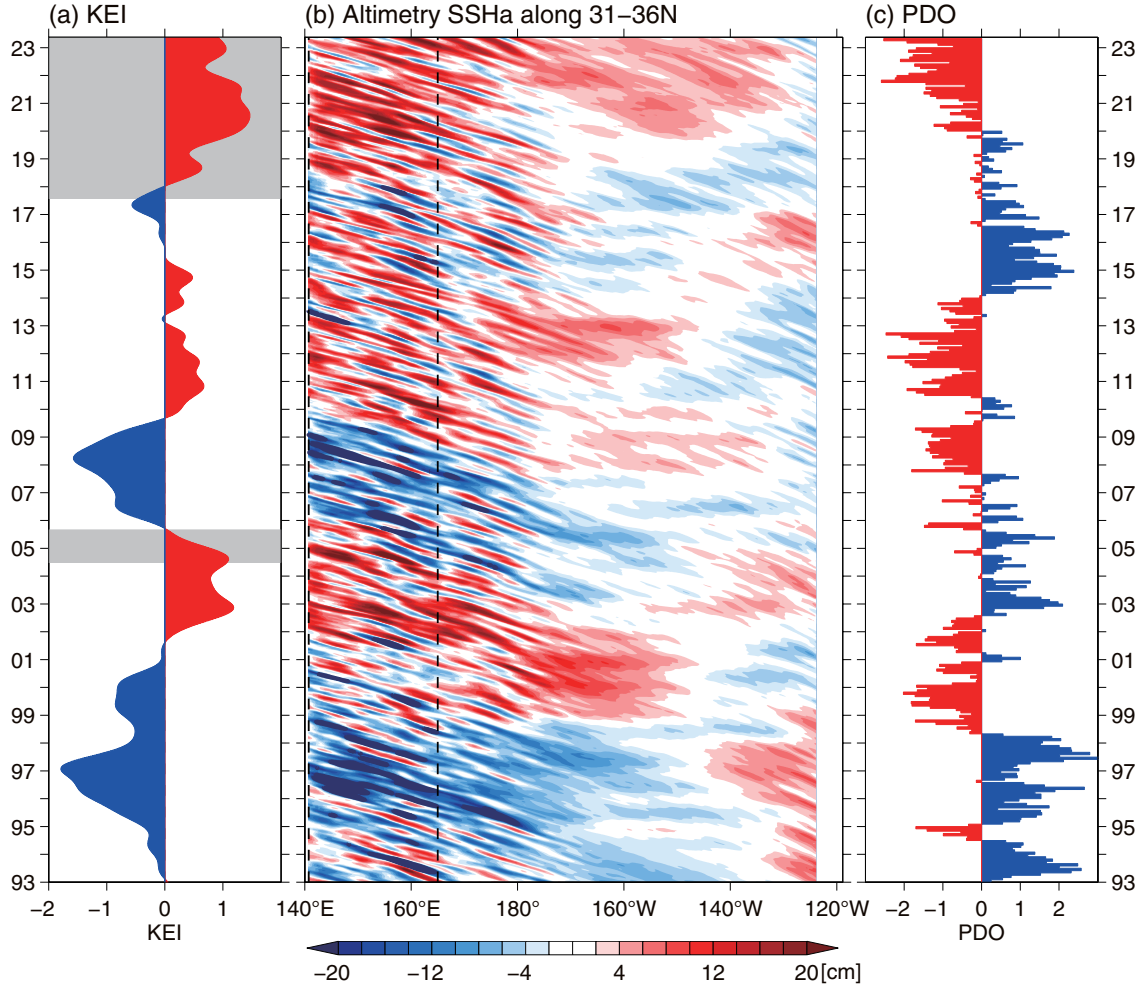

Fig. 12. (a) KE index time series (same as Fig. 11e). (b) Time-longitude plot of SSH anomalies along the 31°-36° N band. Dashed lines denote the RG-box segment. To focus on the regional variability, the 3.3 mm/year global-mean sea level rise trend is removed. (c) PDO index. Adapted from Qiu *et al.* (2023).

(Fig. 13a). The extended KE index reveals that the decadal modulations of the KE dynamical state are not confined to the last 3 decades during which we had satellite altimetry SSH information. To examine how the dominant period of the wind-forced KE variability has modulated over the past century, we plot in Fig. 13b the wavelet power spectrum for the inferred KE index time series. Large-amplitude decadal changes can be seen to have persisted after the mid-1970s. From mid-1940s to mid-1970s, the KE index appears to have two dominant periods: one in the 15 ~ 20-year band and the other in the 4 ~ 6-year band. Note that the short 4 ~ 6-year variability in the KE index was also detected in the eddy-resolving OFES model output of 1955-1975 that was forced by the NCEP-NCAR reanalysis wind stress data (Qiu *et al.*, 2014; their Figure 5a). In between the mid-1920s and mid-1940s, the KE index appears to be dominated by the 10~15-year fluctuations and prior to the mid-1920s, Fig. 13b indicates that the predominant period of the time-varying KE index falls in between 6 and 10 years. It is worth emphasizing that the mid-1920s, mid-1940s, and mid-1970s marked the

three 20th-century climatic regime shifts in the Aleutian Low pressure system over the North Pacific Ocean (Minobe, 1997). The results in Fig. 13b clearly indicate that these regime shifts in the atmospheric forcing field exert a significant impact upon the frequency content of the time-varying KE system.

While our analyses above have focused on the KE variability produced by the wind stress forcing across the North Pacific basin, it is important to emphasize that oceanic nonlinear processes, such as the Kuroshio LM occurrences listed in Fig. 9, can also contribute to the time-varying KE dynamical state. When the Kuroshio south of Japan takes a stationary LM path, the Kuroshio jet overriding the Izu Ridge along ~ 140°E is forced to pass through a deep channel near 34°N with a northeastward angle (see, for example, Fig. 5a in Qiu *et al.*, 2023). Such an orientation by the exiting Kuroshio jet works to guide the upstream KE to flow poleward and favors a stabilized dynamical state of the KE system. In the recent 5 years from 2018 to 2022, Figs.

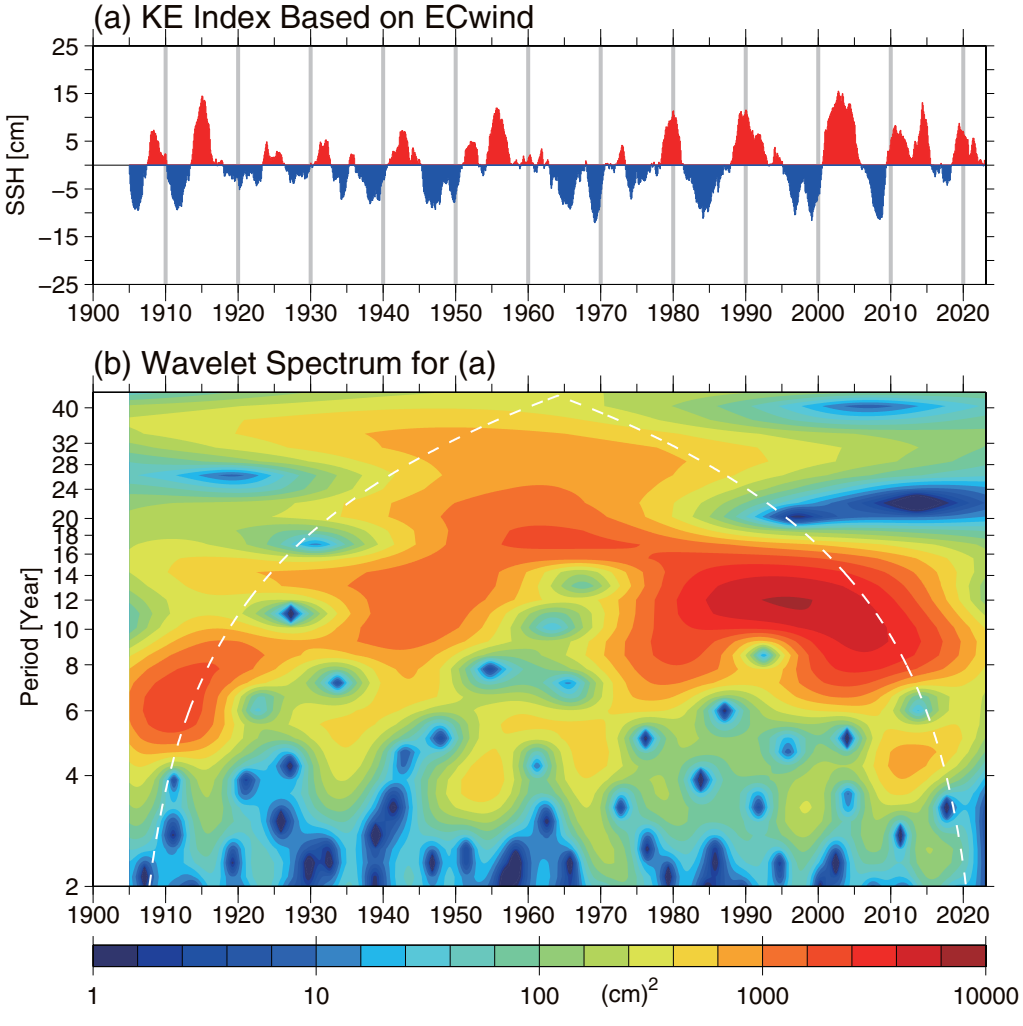

Fig. 13. (a) KE index time series based on the SSH anomalies in the 31°-36°N and 140°-165°E box predicted by the 1.5-layer reduced-gravity model forced by the merged ERA-20C and ERA-5 wind stress data. (b) Wavelet power spectrum for the time series of (a).

11f and 11g indicate that compared to the wind-forced KE index with an average amplitude of ~ 5 cm, the observed KE index amplitude reaches to ~ 10 cm. This discrepancy is due to the prolonged 2017 Kuroshio LM that has forced the KE path to shift poleward, leading to an increase in the observed KE index (see Figs. 10 and 11c). In other words, the highly-stable KE dynamical state observed in the recent 5 years is a combined response to the occurrence of the Kuroshio LM west of the Izu Ridge and the forcing by the interior wind stresses across the North Pacific basin.

As the KE dynamical state vacillates between the stable and unstable states, the regional sea level/circulation patterns and watermass properties can undergo significant changes. For example, as the KE system stabilizes, the wintertime mixed layer depth south of the KE jet tends to deepen due to favorable pre-conditioning in the upper ocean stratification. This can facilitate the formation of Subtropical Mode Water (STMW) (e.g., Qiu and Chen 2006; Qiu *et al*. 2007a; Oka and Qiu, 2012; Oka *et al.*, 2015; Sugimoto and Kako, 2016). When the KE is in a stable dynamical state with a low upstream (140°-153°E) eddy activity, there is a tendency for its downstream (east of 153°E) eddy activity to increase (Qiu and Chen, 2011; Yang *et al.*, 2018). Due to this regional EKE seesaw, the Central Mode Water (CMW) formation in the downstream KE region exhibits an opposite decadal oscillation from that of the STMW (Oka *et al.*, 2012). In the sub-surface layer below the main thermocline, the North Pacific Intermediate Water (NPIW) appears and is characterized as a regional salinity minimum layer (see Qiu, 1995 and references therein). When the KE is in a stable dynamical state, the high eddy activity in the downstream KE region has been observed to enhance the transfer of low-salinity NPIW from the western subarctic gyre into the western subtropical gyre (Qiu and Chen, 2011). In addition to the watermass variations, the decadal KE variability also exerts impact upon the regional sea level signals. As the KE system becomes stable and migrates poleward, there is tendency for coastal sea level around Japan to increase as a result of direct impact by the KE jet migration and of the subsequent propagation of coastally-trapped waves (Sasaki *et al.*, 2014; Usui and Ogawa, 2022). It is worth emphasizing that the large-scale sea level fluctuations associated with the KE system is generated *both* by the basin-scale wind stress forcing and by the eddy-eddy interactions along the KE jet (Qiu *et al.*, 2015). When the eddy activity increases decadally along the KE jet, the enhanced eddy-eddy interaction can produce dipolar sea level anomalies with positive (negative) sea levels south (north) of the KE jet.

We have in section 3 mentioned that the low-frequency STCC eddy activity modulations can regulate the initiation of Kuroshio LMs south of Japan. By analyzing the eddy-resolving altimeter-measured SSH data covering the 2004-05 versus 2017-present LM events, Qiu *et al.* (2023) found recently that the stability of the wind-forced KE dynamical state played an important role in affecting the LM durations. Compared to the 2004-05 LM event which was short-lived due to the stable-to-unstable transition by the KE in 2005, the highly stable KE in the past 5 years (see Fig. 11e) not only minimized westward eddy perturbations from disrupting the upstream Kuroshio path, its strengthened southern recirculation gyre further helped to anchor the Kuroshio across the Izu Ridge.

5. Mid-Latitude Ocean-Atmosphere Coupling

Like other extratropical western boundary currents, the Kuroshio/KE transport a great amount of warmer tropical water poleward, providing a source of heat and moisture for the midlatitude atmosphere (Kelly *et al.*, 2010). This source of oceanic heat/moisture has been demonstrated by many recent studies to help maintain the lower tropospheric baroclinicity and anchor the extratropical stormtracks (Nakamura *et al.*, 2004; Minobe

et al., 2008; Kwon *et al.*, 2010; Small *et al.*, 2014; Masunaga *et al.*, 2016; Ma *et al.*, 2016; Bishop *et al.*, 2017). Many data analysis studies in the past decades have examined the impact of SST changes in the KE region on the atmospheric circulation across the midlatitude North Pacific basin (Frankignoul and Sennechael, 2007; Qiu *et al.*, 2007b, 2014; Frankignoul *et al.*, 2011; Taguchi *et al.*, 2012; Smirnov *et al.*, 2015; Ma *et al.*, 2015; O'Reilly and Czaja, 2014; Revelard *et al.*, 2016). A consistent feature resulting from these analyses is that when the KE

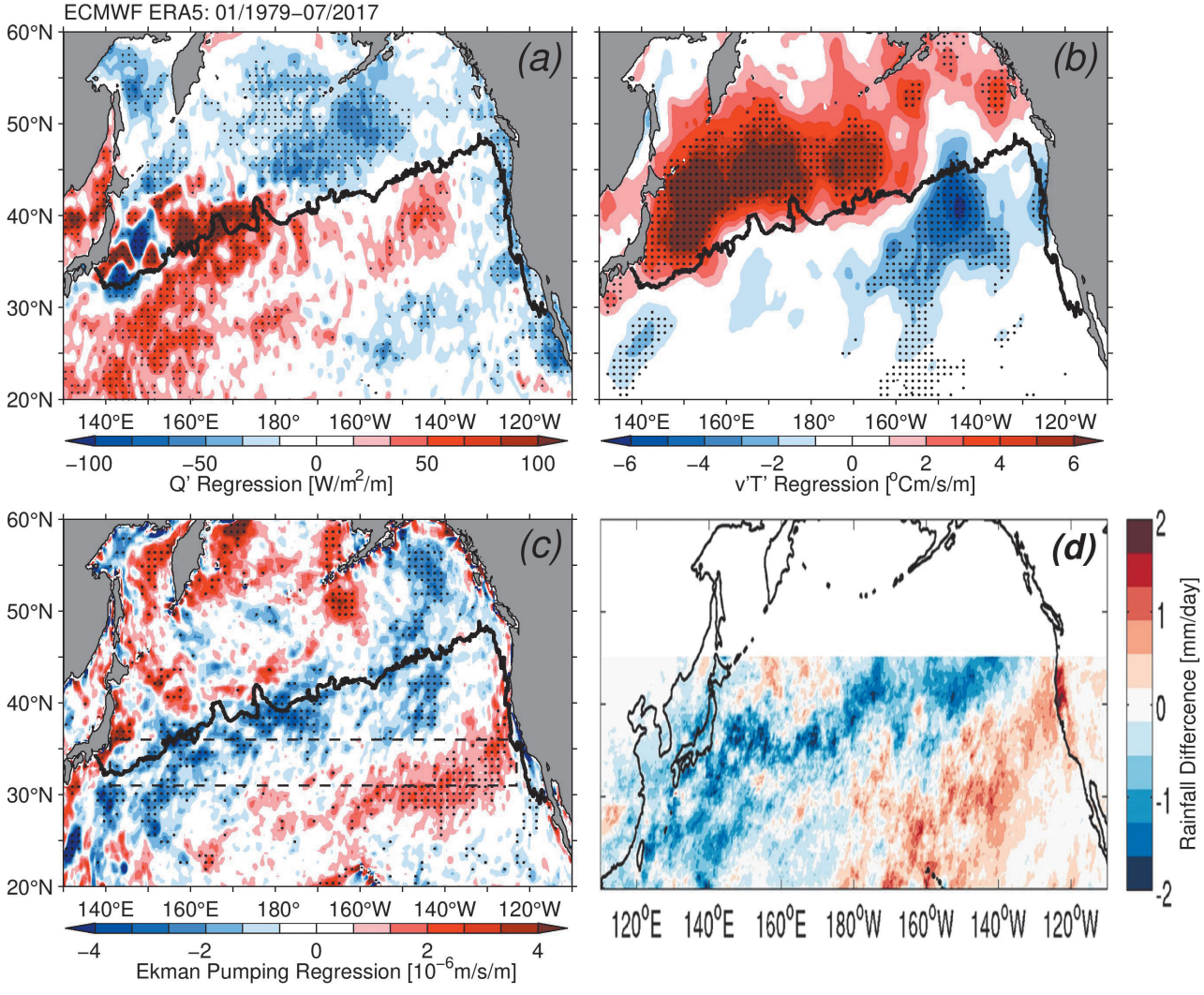

Fig. 14. (a) Regression coefficient between the surface turbulent heat flux anomaly field and the KE index of Jan 1979–Jul 2017 with the former lagging the latter by 2 months. (b) As in (a), but for the 2–8-day band-passed meridional transient eddy temperature flux anomaly field at the 850-hPa level. (c) As in (a), but for the Ekman pumping velocity (W_{Ek}) anomaly field. In all figures, the thick black contour denotes the time-mean $W_{Ek} = 0$ line and stippled areas indicate where the statistical significance exceeds the 90% confidence level based on Monte Carlo simulations. Dashed box in (c) indicates the 31°–36°N band where the Ekman pumping forcing impacts the KE dynamic state. (a)–(c) are adapted from Qiu *et al.* (2020). (d) Difference of TRMM winter season (NDJFM) mean rainfall (mm/d) between stable and unstable KE dynamical state years. Adapted from Ma *et al.* (2015).

dynamical state is stable, increased surface turbulent heat fluxes tend to emit from ocean to atmosphere along the poleward-shifted KE path (Fig. 14a; defined positive from ocean to atmosphere). This enhanced turbulent heat flux forcing results in northward migration/amplification of the extratropical stormtracks as can be inferred from the lower tropospheric transient eddy $\langle v'T' \rangle$ distributions shown in Fig. 14b.

Notice that the time-mean stormtracks follow roughly the W_{Ek} = 0 line denoted by the thick black contour in Fig. 14b. This line is tilted SW-NE across the North Pacific basin due to the combined orographic constraint and diabatic oceanic forcing (Wilson *et al.*, 2009). When the stormtracks migrate northward during the stable KE state, a negative W_{Ek} anomaly band appears that straddles the time-mean W_{Ek} = 0 line (Fig. 14c). South of this band, the W_{Ek} anomalies turn positive because the northward wind system migration brings in stronger, subtropical-origin, negative W_{Ek} signals from the south. As a consequence, anomalous W_{Ek} in the 31°-36° N band of the eastern North Pacific becomes positive. For the lower atmosphere, this positive W_{Ek} anomaly brings about enhanced regional rainfall over the eastern North Pacific (Fig. 14d; Ma *et al.*, 2015). For the upper ocean, this leads to regional Ekman flux divergence and negative SSH anomalies in the eastern North Pacific Ocean. When these wind-forced negative SSH signals propagate westward into the KE region with a

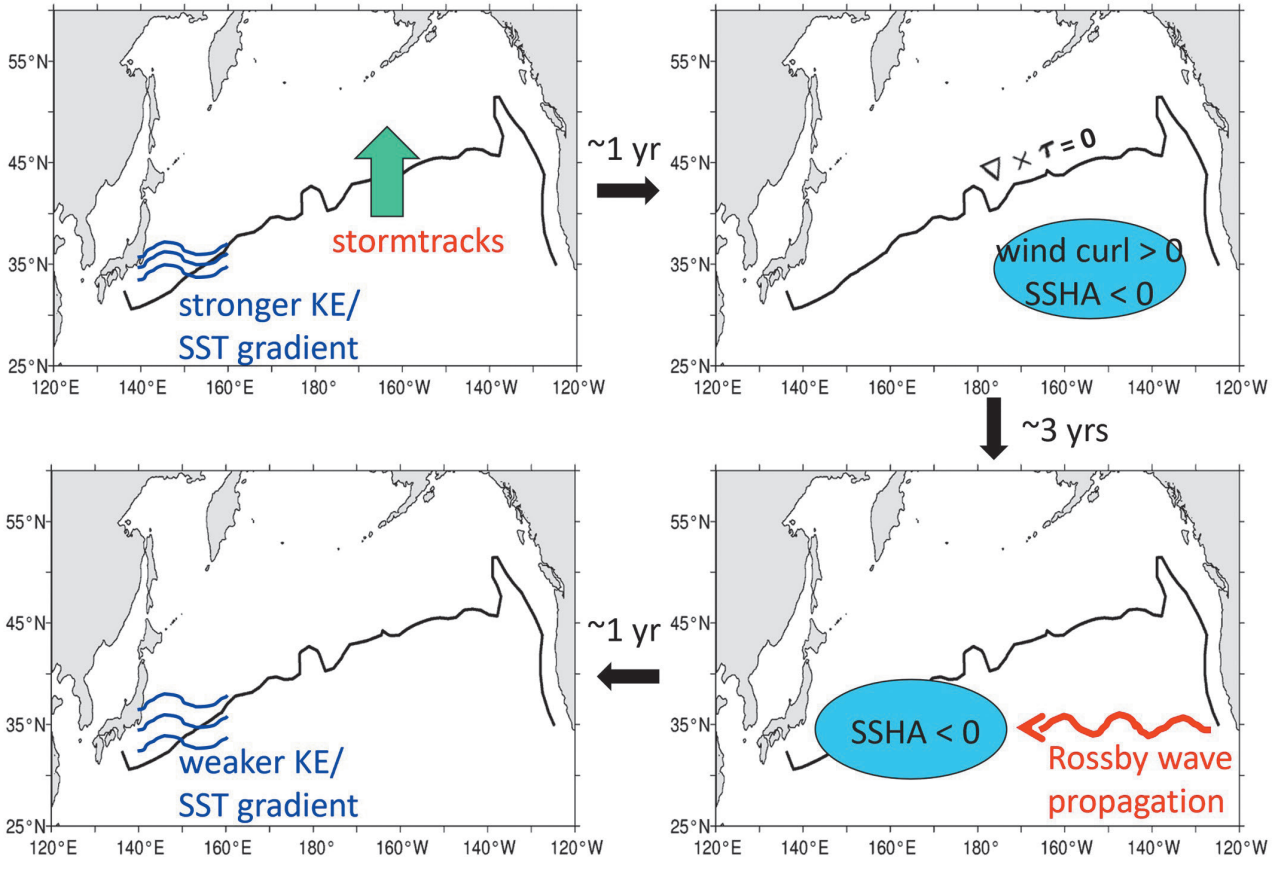

Fig. 15. Schematic of the ocean-atmosphere coupled mode due to delayed negative feedback in the midlatitude North Pacific basin. Here, the black line denotes the mean zero-wind-stress-curl line and corresponds to the mean position of the North Pacific storm tracks.

delay of ~ 3 years, they work to weaken the southern recirculation gyre, shifting the KE jet southward to override the shallow Izu Ridge, and transforming the KE system to an unstable dynamical state. Once the KE system switches to its unstable state, the reverse of the atmospheric responses depicted in Fig. 14 takes place and a dynamical state transition to a stable state occurs following a delayed oceanic adjustment. Although the KE-induced basin-scale atmosphere response is weak in comparison with the internal atmospheric fluctuations (typically at 10 ~ 15% level for the interannual and decadal signals; Qiu *et al.*, 2007b), this ocean-to-atmosphere feedback loop provides a negative feedback mechanism that was argued by several recent studies to explain the enhanced decadal variability observed in the extratropical North Pacific Ocean and atmosphere (see Fig. 15 for a schematic; Qiu *et al.*, 2014; Smirnov *et al.*, 2015; Na *et al.*, 2018).

Instead of invoking the stormtrack migration, Joh and Di Lorenzo (2019) have found recently that the decadally-varying KE can induce an eastern Pacific wind stress curl response that projects on atmospheric forcing of the Pacific meridional mode (PMM; Chiang and Vimont 2004). Specifically, when it is in a stable state, the KE-induced positive W_{Ek} anomaly shown in Fig. 14c in the 25°-35°N band of the eastern North Pacific projects to the positive PMM forcing pattern. This PMM forcing can activate the central tropical Pacific El Niño-Southern Oscillation (CP-ENSO), which in turn can strengthen a positive PDO forcing through atmospheric bridge, generating the negative SSH anomalies in the eastern North Pacific and altering the KE to an unstable state after these wind-forced SSH anomalies propagate into the KE region.

6. Summary

Throughout this article, we have emphasized that although individual circulation systems in the North Pacific subtropical gyre have their unique properties and distinct time-varying signals, it is dynamically beneficial to consider them in an inter-connected way through external forcings or mutual interactions. As summarized schematically in Fig.16, an important external forcing that is common to the NEC, the upstream Kuroshio along the western boundary, the STCC east of Taiwan, the bimodal Kuroshio paths south of Japan, and the Kuroshio Extension in the open North Pacific, is the low-frequency surface wind variability modulated by the Pacific Decadal Oscillations. Specifically,

- The PDO-related wind forcing has an imprint on the western tropical Pacific Ocean. With its center of action located long 9°-16°N, this decadal forcing after 1990s alters effectively the NEC's bifurcation latitude along the Philippine coast: during the positive-(negative-)phased PDO forcing, the NEC bifurcation tends to migrate poleward (equatorward). The impact by the migrating NEC can permeate into the marginal Indonesian Sea, the South China and the East Chine Sea by advection or coastal boundary wave guides. By influencing the upstream Kuroshio, the NEC's impact could also be transmitted downstream into the East China Sea, or possibly south of Japan, via advection.

- Through Ekman flux convergence along the central latitudes of the subtropical gyre, the PDO forcing can also effectively modulate the baroclinicity associated with the STCC and its underlying NEC. A positive-phased PDO forcing works to increase the baroclinicity and enhances the eddy kinetic energy level along the STCC band, and vice versa for the negative-phased forcing. An elevated STCC eddy activity not only alters the Kuroshio path and transport east of Taiwan and the Luzon Strait, it also favors initiations of the Kuroshio LM events through the "eddy corridor" east of the Ryukyu Islands.

- With a lead of ~3 years, the PDO-related wind forc-

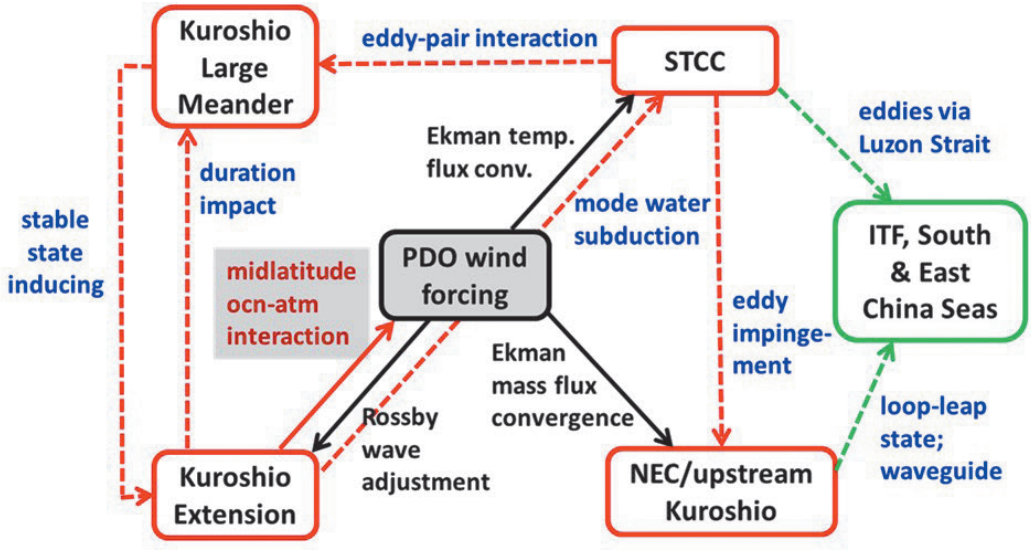

Fig. 16. A schematic summarizing the inter-connected atmospheric forcing and the four circulation subsystems in the wind-driven North Pacific subtropical gyre. Black arrows/labels denote the forcing processes related to PDOs, dashed red arrows denote interactions among the subsystems, dashed green arrows denote impacts on marginal seas, blue labels denote relevant processes, and solid red arrow/label denote ocean's feedback to the atmosphere.

ing can modulate the KE dynamical state effectively, with a positive-(negative-)phased forcing resulting in an unstable (stable) state. In addition, as exemplified by the recent 2017 event, the Kuroshio LM can also trigger a change in the downstream KE dynamical system and the wind-forced changes in the KE system could, in turn, dictate the duration of an existing LM event. As the KE dynamical state fluctuates on decadal timescales, it not only can affect the water mass properties and sea levels in the neighboring areas; through subduction and ventilation from the surface mixed layer into the main thermocline, the KE-induced mode water variations can also alter the subsurface potential vorticity structures along the interior paths, influencing potentially the long-term stability signals of the STCC.

• While *all* the circulation systems described in this article are subject to the PDO forcing, it is equally important to recognize that via turbulent heat flux release, the low-frequency Kuroshio/KE variations could feedback to the overlying atmospheric storm-tracks and form coupled feedback loops. Due to ocean's slow response and larger heat capacity, such coupled feedback loops can enhance the longer-timescale variance in the midlatitude North Pacific climate system. With the longer observational data/reanalysis products and high-resolution coupled general circulation model simulations become available, more insights in this research area will undoubtedly be further explored and advanced in future.

Acknowledgements

I am extremely honored and humbled to be bestowed the 2019 Japan Oceanographic Society (JOS) Award. I want to thank sincerely the nominating colleagues and the JOS Award Selection Committee members. Receiving this highly prestigious award means greatly to me when I look back at my educational career as an undergraduate, a master course, and a doc-

tor course student from Kyoto University. While in Kyoto during 1980–1990, I had been tremendously fortunate to be mentored by Professors Hideaki Kunishi and Norihisa Imasato whose sincere generosity and academic rigor had a forever impact upon me. I was also very lucky to be surrounded by a great number of fellow graduate students in Kyoto and in JOS who had influenced me not only professionally, but also culturally and humanly. After leaving Japan for US in 1990, I had again been exceptionally fortunate to meet my postdoc advisors, Drs. Terry Joyce and Kathie Kelly, at Woods Hole Oceanographic Institution, whose insightful guidance and inspiring integrity had allowed me to blossom under the new research environment in US. Finally, I want to express my sincere gratitude to all my colleagues at the Department of Oceanography, University of Hawaii at Manoa, and all JOS colleagues for their long-standing collaborations, collegiality, and friendship throughout my career.

References

Andres, M., J. H. Park, M. Wimbush, X. H. Zhu, K. I. Chang, and H. Ichikawa (2008): Study of the Kuroshio/Ryukyu Current System based on satellite-altimeter and in situ measurements. *J. Oceanogr.*, **64**, 937–950.

Bishop, S. P., R. J. Small, F. O. Bryan, and R. A. Tomas (2017): Scale dependence of mid-latitude air-sea interaction. *J. Climate*, **30**, 8207–8221.

Capotondi, A., and B. Qiu (2023): Decadal variability of the Pacific overturning circulation and the role of local wind forcing. *J. Climate*, **36**, 1001–1015.

Ceballos, L., E. Di Lorenzo, C. D. Hoyos, N. Schneider, and B. Taguchi (2009): North Pacific Gyre Oscillation synchronizes climate variability in the eastern and western boundary current systems. *J. Climate*, **22**, 5163–5174.

Chelton, D.B., R. A. de Szoeke, M. G. Schlax, K. E. Naggar, and N. Siwertz (2008): Geographical variability of the first baroclinic Rossby radius of deformation. *J. Phys. Oceanogr.*, **28**, 433–460.

Chelton, D. B., M. G. Schlax, and T. M. Samelson (2011): Global observations of nonlinear mesoscale eddies. *Prog. Oceanogr.*, **91**, 167–216, https://doi.org/10.1016/j.pocean.2011.01.002.

Chiang, J. C. H., and D. J. Vimont, 2004: Analogous Pacific and Atlantic meridional modes of tropical atmosphere-ocean variability. *J. Climate*, **17**, 4143–4158, https://doi.org/10.1175/JCLI4953.1.

Ferrari, R., and C. Wunsch (2009): Ocean circulation kinetic energy: Reservoirs, sources, and sinks. *Ann. Rev. Fluid Mech.*, **41**, 253–282, DOI:10.1146/ANNUREV.FLUID.40.111406.102139.

Frankignoul, C., and N. Sennechael (2007): Observed influence of North Pacific SST anomalies on the atmospheric circulation. *J. Climate*, **20**, 592–606.

Frankignoul, C., N. Sennechael, Y.-O. Kwon, and M. A. Alexander (2011): Influence of the meridional shifts of the Kuroshio and the Oyashio Extensions on the atmospheric circulation. *J. Climate*, **24**, 762–777.

Gilson, J., and D. Roemmich (2002): Mean and temporal variability in Kuroshio geostrophic transport south of Taiwan (1993–2001). *J. Oceanogr.*, **58**, 183–195.

Gordon, A. L., P. Flament, C. Villanoy, and L. Centurioni (2014), The nascent Kuroshio of Lamon Bay, *J. Geophys. Res. Oceans*, **119**, 4251–4263, doi:10.1002/2014JC009882.

Hsin, Y.-C., B. Qiu, T.-L. Chiang, C.-R. Wu (2013): Seasonal to interannual variations in the intensity and central position of the surface Kuroshio east of Taiwan. *J. Geophys. Res.*, **118**, doi:10.1002/jgrc.20323.

Hu, D., L. Wu, W. Cai, A. S. Gupta, A. Ganachaud, B. Qiu, A. L. Gordon, X. Lin, Z. Chen, S. Hu, G. Wang, Q. Wang, J. Sprintall, T. Qu, Y. Kashino, F. Wang, and W. S. Kessler (2015): Pacific western boundary currents and their roles in climate. *Nature*, **522**, 299–308, https://doi.org/10.1038/nature14504.

Ichikawa, H., H. Nakamura, A. Nishina, and M. Higashi (2004): Variability of north-eastward current southeast of northern Ryukyu Islands. *J. Oceanogr.*, **60**, 351–363.

Imawaki, S., A.S. Bower, L. Beal, and B. Qiu (2013): Western Boundary Currents. In *Ocean Circulation and Climate - A 21st Century Perspective*, 2nd Edition, G. Siedler, S.M. Griffies, W.J. Gould and J. Church (eds.); Academic Press, pp. 305–338.

Jousset S., S. Mulet, J. Wilkin, E. Greiner, G. Dibarboure, and N. Picot (2022): New global Mean Dynamic Topography CNES-CLS-22 combining drifters, hydrological profiles and High Frequency radar data. OSTST 2022, https://doi.org/10.24400/527896/a03-2022.3292.

Joh, Y., and E. Di Lorenzo (2019): Interactions between Kuroshio Extension and Central Tropical Pacific lead to preferred decadal timescale oscillations in Pacific climate. *Sci. Report*, **9**, 13558.

Kawabe, M. (1995): Variations of current path, velocity, and volume transport of the Kuroshio in relation with the large meander. *J. Phys. Oceanogr.*, **25**, 3103–3117.

Kelly, K.A., R.J. Small, R. M. Samelson, B. Qiu, T. M. Joyce, Y.-O. Kwon, and M.F. Cronin (2010): Western boundary currents and frontal air-sea interaction: Gulf Stream and Kuroshio Extension. *J. Climate*, **23**, 5644–5667.

Kida, S., and Co-authors (2015). Oceanic fronts and jets around Japan: A review. *J. Oceanogr.*, **61**, 469–497. https://doi.org/10.1007/s10872-015-0283-7.

Kim, Y., T. Qu, T. Jensen, T. Miyama, H. Mitsudera, H. Kang, and A. Ishida (2004): Seasonal and interannual variations of the North Equatorial Current bifurcation in a high-resolution OGCM. *J. Geophys. Res.*, **109**, C03040, doi:10.1029/2003JC002013.

Kobashi, F., and H. Kawamura (2002): Seasonal variation and instability nature of the North Pacific Subtropical Countercurrent and the Hawaiian Lee Countercurrent. *J. Geophys. Res.*, **107**, C03185, doi:10.1029/2001JC001225.

Kubokawa, A. (1997): A two-level model of subtropical gyre and subtropical countercurrent, *J. Oceanogr.*, **53**, 231–244.

Kwon, Y.-O., M.A. Alenxader, N.A. Bond, C. Frankignoul, H. Nakamura, B.

Qiu, and L. Thompson (2010): Role of the Gulf Stream and Kuroshio-Oyashio systems in large-scale atmosphere-ocean interaction: A review. *J. Climate*, **23**, 3249-3281.

Lien, R.-C., B. Ma, Y.-H. Cheng, C.-R. Ho, B. Qiu, C.M. Lee, and M.-H. Chang (2014): Modulation of Kuroshio transport by mesoscale eddies at the Luzon Strait entrance. *J. Geophys. Res.*, **119**, 2129-2142, doi:10.1002/2013JC009548.

Ma, X., P. Chang, R. Saravanan, R. Montuoro, J.-S. Hsieh, D. Wu, X. Lin, L. Wu, Z. Jing (2015): Distant influence of Kuroshio eddies on North Pacific weather patterns. *Sci. Report*, **5**, 17785.

Ma, X., J. Zhao, P. Chang, X. Liu, R. Montuoro, R.J. Small, F.O. Bryan, R.J. Greatbatch, P. Brandt, D. Wu, X. Lin, and L. Wu (2016): Western boundary currents regulated by interaction between ocean eddies and the atmosphere. *Nature*, **535**, 533-537.

Masunaga, R., H. Nakamura, T. Miyasaka, K. Nishii, and B. Qiu (2016): Interannual modulations of oceanic imprints on the wintertime atmospheric boundary layer under the changing dynamical regimes of the Kuroshio Extension. *J. Climate,* **29**, 3273-3296.

Minobe, S. (1997): A 50-70 year climatic oscillation over the North Pacific and North America. *Geophys. Res. Lett.*, **24**, 683-686.

Minobe, S., A. Kuwano-Yoshida, N. Komori, S.-P. Xie, and R. J. Small (2008): Influence of the Gulf Stream on the troposphere. *Nature*, **452**, 206-209.

Miyazawa, Y., X. Guo, and T. Yamagata (2004): Roles of mesoscale eddies in the Kuroshio paths. *J. Phys. Oceanogr.*, **34**, 2203-2222.

Na, H., K.-Y. Kim, S. Minobe, and Y.N. Sasaki (2018): Interannual to decadal variability of the upper-ocean heat content in the western North Pacific and its relationship to oceanic and atmospheric variability. *J. Climate*, **31**, 5107-5125.

Nakamura, H., T. Sampe, Y. Tanimoto, and A. Shimpo (2004): Observed associations among storm tracks, jet streams and midlatitude oceanic fronts. *Earth's Climate: The Ocean-Atmosphere Interaction*. Geophys. Monogr., **147**, Amer. Geophys. Union, 329-346.

Nan, F., H. Xue, F. Chai, D. Wang, F. Yu, M. Shi, P. Guo, and P. Xiu, Peng (2013): Weakening of the Kuroshio intrusion into the South China Sea over the past two decades. *J. Climate*, **26**, 10.1175/JCLI-D-12-00315.1.

Nonaka, M., H. Sasaki, M. Taguchi, and N. Schneider (2020): Atmospheric-driven and intrinsic interannual-to-decadal variability in the Kuroshio Extension jet and eddy activities. *Front. Mar. Sci.* **7**: 547442. doi: 10.3389/fmars.2020.547442.

Oka, E., and B. Qiu (2012): Progress of North Pacific mode water research in the past decade. *J. Oceanogr.*, **68**, 5-20.

Oka, E., B. Qiu, S. Kouketsu, K. Uehara, and T. Suga (2012): Decadal seesaw of the Central and Subtropical Mode Water formation associated with the Kuroshio Extension variability. *J. Oceanogr.*, **68**, 355-360.

Oka, E., B. Qiu, Y. Takatani, K. Enyo, D. Sasano, N. Kosugi, M. Ishii, T. Nakano, and T. Suga (2015): Decadal variability of Subtropical Mode Water subduction and its impact on biogeochemistry. *J. Oceanogr.*, **71**, 389-400.

O'Reilly, C.H., and A. Czaja (2014): The response of the Pacific storm track and atmospheric circulation to Kuroshio Extension variability. *Quart. J. Royal Meteoro. Soc.*, doi:10.1002/qj.2334.

Pierini, S. (2014): Kuroshio Extension bimodality and the North Pacific Oscillation: A case of intrinsic variability paced by external forcing. *J. Climate*, **27**, 448-454.

Qiu, B. (1995): Why is the North Pacific Intermediate Water confined on density surfaces around σ_θ = 26.8? *J. Phys. Oceanogr.*, **25**, 168-180.

Qiu, B. (1999): Seasonal eddy field modulation of the North Pacific Subtropical Countercurrent: TOPEX/POSEIDON observations and theory. *J. Phys. Oceanogr.*, **29**, 2471-2486.

Qiu, B. (2002): Large-scale variability in the midlatitude subtropical and subpolar North Pacific Ocean: Observations and causes. *J. Phys. Oceanogr.*, **32**, 353-375.

Qiu, B., and S. Chen (2005): Variability of the Kuroshio Extension jet, recirculation gyre and mesoscale eddies on decadal timescales. *J. Phys. Oceanogr.*, **35**, 2090-2103.

Qiu, B., and S. Chen (2006): Decadal variability in the formation of the North Pacific Subtropical Mode Water: Oceanic versus atmospheric control. *J. Phys. Oceanogr.*, **36**, 1365-1380.

Qiu, B., and S. Chen (2010a): Interannual-to-decadal variability in the bifurcation of the North Equatorial Current off the Philippines. *J. Phys. Oceanogr.*, **40**, 2525-2538.

Qiu, B., and S. Chen (2010b): Interannual variability of the North Pacific Subtropical Countercurrent and its associated mesoscale eddy field. *J. Phys. Oceanogr.*, **40**, 213-225.

Qiu, B., and S. Chen (2010c): Eddy-mean flow interaction in the decadally-modulating Kuroshio Extension system. *Deep-Sea Res. II*, **57**, 1098-1110.

Qiu, B., and S. Chen (2011): Effect of decadal Kuroshio Extension jet and eddy variability on the modification of North Pacific Intermediate Water. *J. Phys. Oceanogr.*, **41**, 503-515.

Qiu, B., and S. Chen (2012): Multi-decadal sea level and gyre circulation variability in the northwestern tropical Pacific Ocean. *J. Phys. Oceanogr.*, **42**, 193-206.

Qiu, B., and S. Chen (2013): Concurrent decadal mesoscale eddy modulations in the western North Pacific subtropical gyre. *J. Phys. Oceanogr.*, **43**, 344-358.

Qiu, B., and S. Chen (2021): Revisit of the occurrence of the Kuroshio large meander south of Japan. *J. Phys. Oceanogr.*, **51**, 3679-3694.

Qiu, B., S. Chen, B. Powell, P.L. Colin, D.L. Rudnick, and M.C. Schonau (2019): Nonlinear short-term upper ocean circulation variability in the tropical western Pacific. *Oceanography*, **32**(4), 22-31.

Qiu, B., S. Chen, and P. Hacker (2007a): Effect of mesoscale eddies on Subtropical Mode Water variability from the Kuroshio Extension System Study (KESS). *J. Phys. Oceanogr.*, **37**, 982-1000.

Qiu, B., N. Schneider, and S. Chen (2007b): Coupled decadal variability in the North Pacific: An observationally-constrained idealized model. *J. Climate*, **20**, 3602-3620.

Qiu, B., S. Chen, and E. Oka (2023): Why did the 2017 Kuroshio Large Meander become the longest in the past 70 years? *Geophys. Res. Lett.*, **50**, e2023GL103548. https://doi. org/10.1029/2023GL103548.

Qiu, B., S. Chen, N. Schneider, E. Oka, and S. Sugimoto (2020): On reset of the wind-forced decadal Kuroshio Extension variability in late 2017. *J. Climate*, **33**, 10813-10828.

Qiu, B., S. Chen, N. Schneider, and B. Taguchi (2014): A coupled decadal prediction of the dynamic state of the Kuroshio Extension system. *J. Climate*, **27**, 1751-1764.

Qiu, B., S. Chen, L. Wu, and S. Kida (2015): Wind- versus eddy-forced regional sea level trends and variability in the North Pacific Ocean. *J. Climate*, **28**, 1561-1577.

Qiu, B., and R. Lukas (1996): Seasonal and interannual variability of the North Equatorial Current, the Mindanao Current and the Kuroshio along the Pacific western boundary. *J. Geophys. Res.*, **101**, 12,315–12,330.

Revelard, A., C. Frankignoul, N. Sennechael, Y.-O. Kwon, and B. Qiu (2016): Influence of the decadal variability of the Kuroshio Extension on the atmospheric circulation in the cold season. *J. Climate*, **29**, 2123–2144.

Risien, C. M., and D. B. Chelton (2008): A global climatology of surface wind and wind stress fields from eight years of QuikSCAT scatterometer data. *J. Climate*, **38**, 2379–2413.

Roden, G. I. (1980): On the variability of surface temperature fronts in the western Pacific, as detected by satellite, *J. Geophys. Res.*, **85**(C5), 2704–2710, doi:10.1029/JC085iC05p02704.

Roemmich, D., and J. Gilson (2001): Eddy transport of heat and thermocline waters in the North Pacific: A key to interannual/decadal climate variability? *J. Phys. Oceanogr.*, **31**, 675–687.

Sasaki, Y. N., S. Minobe, and Y. Miura (2014): Decadal sea-level variability along the coast of Japan in response to ocean circulation changes. *J. Geophys. Res.*, **119**, 266–275.

Sasaki, Y. N., S. Minobe, and N. Schneider (2013): Decadal response of the Kuroshio Extension jet to Rossby waves: Observation and thin-jet theory. *J. Phys. Oceanogr.*, **43**, 442–456.

Schonau, M.C., D.L. Rudnick, G. Gopalakrishnan, B.D. Cornuelle, and B. Qiu (2022): Mean, annual and interannual circulation and volume transport in the western tropical North Pacific from the Western Pacific Ocean State Estimates (WPOSE). *J. Geophys. Res.*, **126**, doi:10.1029/2021JC018213.

Small, R. J., R. A. Tomas, F. O. Bryan (2014): Storm track response to ocean fronts in a global high-resolution climate model. *Climate Dyn.*, **43**, 805–828.

Smirnov, D., M. Newman, M.A. Alexander, Y.-O. Kwon, and C. Frankignoul (2015): Investigating the local atmospheric response to a realistic shift in the Oyashio sea surface temperature front. *J. Climate*, **28**, 1126–1147.

Stammer D., A. Cazenave, R. M. Ponte, and M. E. Tamisiea (2013): Causes for contemporary regional sea level changes. *Annu. Rev. Mar. Sci.*, **5**, 21–46, doi: 10.1146/annurev-marine-121211-172406.

Stickler, A., S. Brönnimann, M. A. Valente, J. Bethke, A. Sterin, S. Jourdain, E. Roucaute, M. V. Vasquez, D. A. Reyes, R. Allan, and D. Dee (2014): ERA-CLIM: Historical surface and upper-air data for future reanalyses. *Bull. Amer. Meteor. Soc.*, **95**, 1419–1430.

Sugimoto, S., and K. Hanawa (2009): Decadal and interdecadal variations of the Aleutian Low cctivity and their relation to upper oceanic variations over the North Pacific. *J. Meteorol. Soc. Japan*, **87**, 601–614.

Sugimoto S., S. Kako (2016): Decadal variation in winter mixed layer depth south of the Kuroshio Extension and its influence on winter mixed layer temperature. *J. Climate*. **29**, 1237–1252.

Taguchi, B., H. Nakamura, M. Nonaka, N. Komori, A. Kuwano-Yoshida, K. Takaya, and A. Goto (2012): Seasonal evolutions of atmospheric response to decadal SST anomalies in the North Pacific subarctic frontal zone: Observations and a coupled model simulation. *J. Climate,* **25**, 111–139.

Taguchi, B., S.-P. Xie, N. Schneider, M. Nonaka, H. Sasaki, and Y. Sasai (2007): Decadal variability of the Kuroshio Extension: observations and an eddy-resolving model hindcast. J. Climate, **20**, 2357–2377.

Usui, N., H. Tsujino, Y. Fujii, and M. Kamachi (2008): Generation of a trigger meander for the 2004 Kuroshio large meander. *J. Geophys. Res.*, **113**, C01012, doi:10.1029/2007JC004266.

Usui, N., and K. Ogawa (2022): Sea level variability along the Japanese coast forced by the Kuroshio and its extension. *J. Oceanogr.*, **78**, 515–527.

Wang, L.-C., C.-R. Wu, and B. Qiu (2014): Modulation of Rossby waves on the Pacific North Equatorial Current bifurcation associated with the 1976 climate regime shift. *J. Geophys. Res.*, **119**, 6669–6679, doi:10.1002/2014JC010233.

Wilson, C., B. Sinha, and R.G. Williams (2009): The effect of ocean dynamics and orography on atmospheric storm tracks. *J. Climate*, **22**, 3689–3702.

Wu, C.-R., Y.-F. Lin, and B. Qiu (2019): Impact of the Atlantic multidecadal oscillation on the Pacific North Equatorial Current bifurcation. *Sci. Report*, **9**, 2162. http://doi.org/10.1038/s41598-019-38479-w.

Wu, C. R. (2013): Interannual modulation of the Pacific Decadal Oscillation (PDO) on the low-latitude western North Pacific. *Prog. Oceanogr.*, **110**, 49–58.

Yang, H., B. Qiu, P. Chang, L. Wu, S. Wang, Z. Chen, and Y. Yang (2018): Decadal variability of eddy characteristics and energetics in the Kuroshio Extension: Unstable versus stable states. *J. Geophys. Res.*, **123**, http://doi.org/10.1029/2018JC014081.

Yoshida, K., and T. Kidokoro (1967): A subtropical countercurrent in the North Pacific -- An eastward flow near the Subtropical Convergence. *J. Oceanogr. Soc. Japan*, **23**, 88–91.

Zhang, D., T. N. Lee, W. E. Johns, C. T. Liu, and R. Zantopp (2001): The Kuroshio east of Taiwan: modes of variability and relationship to interior ocean mesoscale eddies. *J. Phys. Oceanogr.*, **31**, 1054–1074.

Zhang Z., W. Wang, and B. Qiu (2014): Oceanic mass transport by mesoscale eddies. *Science*, **345**, 322–324, DOI: 10.1126/science.1252418.

Zhang, Z., W. Zhao, J. Tian, and X. Liang (2013): A mesoscale eddy pair southwest of Taiwan and its influence on deep circulation. *J. Geophys. Res. Oceans*, **118**, 6479–6494, doi:10.1002/2013JC008994.

Zhuang, W., B. Qiu, and Y. Du (2013): Low-frequency western Pacific Ocean sea level and circulation changes due to the connectivity of the Philippine archipelago. *J. Geophys. Res.*, **118**, 6759–6773, doi:10.1002/2013JC009376.

北太平洋の表層循環とその変動に関する観測的・理論的研究*

Bo Qiu †

要　旨

本論文では，風成循環である北太平洋亜熱帯循環系の西部に存在する 4 つの主要な海流系，すなわち，亜熱帯循環の南縁にある北赤道海流，亜熱帯循環の中心緯度を横切る亜熱帯反流，大蛇行と非大蛇行の流路をとる日本南岸の黒潮，そして北太平洋の内部領域へと流れ込む黒潮続流について，説明する。これらの海流系それぞれは固有の特性と時間変動シグナルを有するが，それらを別々にではなく，外部強制や相互作用を通じて互いに関連させて論じることが，海流系の力学的理解に有益であることが示される。さらに，低周波の黒潮 / 黒潮続流変動が，太平洋十年規模振動に関連するような大気強制に対する受動的な応答ではなく，その海域を覆う大気のストームトラックに影響することによって，中緯度北太平洋における大気海洋系の十年変動を増幅する結合フィードバックループを形成可能であることの重要性を示す。

キーワード：風強制よる海洋循環変動，太平洋 10 年規模振動，中緯度海洋大気結合，負の遅延フィードバック

＊　2023 年 6 月 14 日受領　2023 年 7 月 12 日受理

†　Department of Oceanography, University of Hawaii at Manoa, 1000 Pope Rd., Honolulu, HI 96822, USA
e-mail : bo@soest.hawaii.edu